การเคลือบพอลิอิเล็กโตรไลต์หลายชั้นบนเยื่อเลือกผ่านเส้นใยอิเล็กโตรสปัน
เซลลูโลสอะซิเตตสำหรับการแยกเกลือ

นางสาววทัตตา ฤทธิ์เจริญ

POLYELECTROLYTE MULTILAYER COATING ON ELECTROSPUN CELLULOSE
ACETATE FIBROUS MEMBRANE FOR DESALINATION

Miss Watadta Ritcharoen

A Thesis Submitted in Partial Fulfillment of the Requirements
for the Degree of Master of Engineering Program in Chemical Engineering
Department of Chemical Engineering
Faculty of Engineering
Chulalongkorn University
Academic Year 2007

Thesis Title   POLYELECTROLYTE MULTILAYER COATING ON
                ELECTROSPUN CELLULOSE ACETATE FIBROUS
                MEMBRANE FOR DESALINATION
By   Miss Watadta Ritcharoen
Field of study Chemical Engineering
Thesis Advisor Associate Professor Prasert Pavasant, Ph.D.
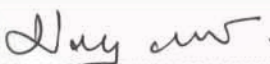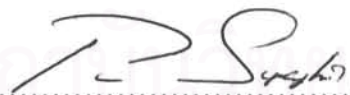Thesis Co-advisor   Associate Professor Pitt Supaphol, Ph.D.

Accepted by the Faculty of Engineering, Chulalongkorn University in Partial Fulfillment of the Requirements for the Master's Degree
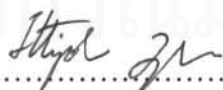
.....................................Dean of the Faculty of Engineering

(Associate Professor Boonsom Lerdhirunwong, Dr.Ing.)

THESIS COMMITTEE

.....................................Chairman

(Associate Professor Seeroong Prichanont, Ph.D.)

.....................................Thesis Advisor

(Associate Professor Prasert Pavasant, Ph.D.)

.....................................Thesis Co-advisor

(Associate Professor Pitt Supaphol, Ph.D.)

.....................................Member

(Associate Professor Ittipol Jangchud, Ph.D.)

.....................................Member

(Sorada Kanokpanont, Ph.D.)

วทัตตา ฤทธิ์เจริญ : การเคลือบพอลิอิเล็กโตรไลต์หลายชั้นบนเยื่อเลือกผ่านเส้นใยอิเล็กโตร
สปันเซลลูโลสอะซิเตตสำหรับการแยกเกลือ (POLYELECTROLYTE
MULTILAYER COATING ON ELECTROSPUN CELLULOSE ACETATE
FIBROUS MEMBRANE FOR DESALINATION) อ. ที่ปรึกษา: รศ.ดร.ประเสริฐ
ภวสันต์, อ. ที่ปรึกษาร่วม: รศ.ดร. พิชญ์ ศุภผล, 64 หน้า.

การเคลือบหลายชั้นของพอลิอิเล็กโตรไลต์หลายชั้น โดยอาศัยแรงทางทางประจุของพอลิอิ-
เล็กโตรไลต์ประจุบวก คือ ไคโตซาน กับพอลิอิเล็กโตรไลต์ประจุลบคือ โซเดียมอัลจิเนต และ พอ-
ลิสไตรีนซัลโฟเนต บนเส้นใยอิเล็กโตรสปันเซลลูโลสอะซิเตต ได้สำเร็จ โดยศึกษาสัณฐานวิทยา
ของเยื่อเลือกผ่านคอมโพสิทด้วย กล้องจุลทรรศน์อิเล็กตรอนแบบส่องกราด ซึ่งสัณฐานวิทยาของ
เยื่อเลือกผ่านที่เคลือบด้วย ไคโตซาน/โซเดียมอัลจิเนต มีความเรียบมากกว่า เยื่อเลือกผ่านที่เคลือบ
ด้วย ไคโตซาน/พอลิสไตรีนซัลโฟเนต การวิเคราะห์หมู่ฟังก์ชันที่ชั้นบนสุดของเยื่อเลือกผ่านพบว่า
หมู่ฟังก์ชันคาร์บอกซิล (1,596 และ 1,411 ต่อเซนติเมตร) และ ซัลโฟนิก (1,007 และ 1,035 ต่อ
เซนติเมตร) สำหรับ โซเดียมอัลจิเนต และ พอลิสไตรีนซัลโฟเนต ตามลำดับ ส่วนหมู่ฟังก์ชันอะมิ-
โนของไคโตซานปรากฏเพียงเล็กน้อย เทคนิคเอ็กซเรย์โฟโตอิเล็กตรอนสเปกโตรสโคปี ยืนยันผล
การยึดติดของไคโตซานบนพื้นผิวของเมมเบรน เยื่อเลือกผ่านถูกวิเคราะห์สำหรับการซึมผ่านน้ำ
พบว่า ค่าฟลักซ์น้ำลดลง เมื่อจำนวนชั้นเคลือบมากขึ้น ซึ่งมีค่า 60 ลิตรต่อตารางเมตรต่อชั่วโมง เมื่อ
เคลือบพอลิอิเล็กโตรไลต์ 15 คู่ชั้น และ 40 ลิตรต่อตารางเมตรต่อชั่วโมง เมื่อเคลือบพอลิอิเล็กโตร
ไลต์ 25 คู่ชั้น สำหรับผลของการแยกเกลือโซเดียมคลอไรด์ พบว่า ฟลักซ์ของสารละลายต่ำกว่า
ฟลักซ์น้ำ เนื่องมาจากผลของความดันออสโมติก และ ฟลักซ์ของสารละลายลดลง เมื่อความเข้มข้น
ของสารละลายโซเดียมคลอไรด์เพิ่มขึ้น สำหรับค่าการกักกันโซเดียมคลอไรด์ พบว่า มีค่าเพิ่มขึ้น
เมื่อจำนวนชั้นเคลือบมากขึ้น ซึ่งระดับค่าการกักกันของโซเดียมคลอไรด์ ในงานวิจัยนี้อยู่ในช่วง 15
เปอร์เซ็นต์ สำหรับเคลือบพอลิอิเล็กโตรไลต์ 25 คู่ชั้น และ 6 เปอร์เซ็นต์ สำหรับเคลือบพอลิอิเล็ก
โตรไลต์ 15 คู่ชั้น

ภาควิชา.........วิศวกรรมเคมี..................... ลายมือชื่อนิสิต............วทัตตา ฤทธิ์เจริญ................

สาขาวิชา.......วิศวกรรมเคมี..................... ลายมือชื่ออาจารย์ที่ปรึกษา........................

ปีการศึกษา ...2550.........................ลายมืออาจารย์ที่ปรึกษาร่วม........................

4870446621: MAJOR   CHEMICAL ENGINEERING
KEY WORD: POLYELECTROLYTE MULTILAYER / CELLULOSE ACETATE / ELECTROSPUN / WATER FLUX / NaCl REJECTION

WATADTA RITCHAROEN: POLYELECTROLYTE MULTILAYER COATING ON ELECTROSPUN CELLULOSE ACETATE FIBROUS MEMBRANE FOR DESALINATION. THESIS ADVISOR: ASSOC. PROF. PRASERT PAVASANT, PH.D., THESIS CO-ADVISOR: ASSOC. PROF. PITT SUPAPHOL, PH.D., 64 pp.

Electrostatic multilayers of chitosan (CHI) with sodium alginate (SA) and poly (styrene sulfonate) sodium salt (PSS) were alternatively coated on electrospun cellulose acetate (CA) fiber mat. Morphologies of the composite membranes were characterized by scanning electron microscope (SEM). The morphology of the CHI/SA coated membrane was denser than the CHI/PSS coated membrane. Functional groups of the top layers were quite clear with carboxyl (1,596 and 1,411 cm^{-1}) and sulfonic (1,007   and 1,035 cm^{-1}) for SA and PSS, respectively. Amino groups of CHI were only presented in slight quantity. X-ray photoelectron spectroscopy (XPS) confirmed the deposition of amino groups from CHI on multilayer membrane surface. These membranes were characterized for its pure water permeability. It was found that the flux of water decreased with increasing the number of bilayers. The pure water flux was in the range of 60 L m^{-2} h^{-1} for 15 bilayers and 40 L m^{-2} h^{-1} for 25 bilayers. The sodium chloride (NaCl) solution flux was lower than the pure water flux due to the effect of osmotic pressure, and this flux decreased with increasing NaCl concentration. The rejection of NaCl increased substantially with the number of bilayers of the polyelectrolytes multilayers. The level of NaCl rejection from this work was in the range of 15 % for 25 bilayers and 6 % for 15 bilayers.

Department…..Chemical Engineering…   Student's signature…………………………

Field of study...Chemical Engineering…   Advisor's signature ……………………

Academic year …2007………………...   Co-advisor's signature………………………

ACKNOWLEDGEMENTS

CONTENTS

LIST OF TABLES

LIST OF FIGURES

CHAPTER I

INTRODUCTION

1.1 Motivations

Membrane desalination is typically achieved using nanofiltration (NF) or reverse osmosis (RO) processes. These processes require dense or small porous membranes, thus the development of materials providing improved water flux, salt rejection and low operating pressure is significant for actual applications. Composite membranes have been developed with the purposes of reducing of membrane resistance and increasing flux. The composite morphology often consists of thin top layer acting as active separation layer coated onto a porous, low resistance, supporting membrane. The performance of membrane can be improved by surface modifications. Some examples include multiple polyelectrolyte surface modification which resulted in a dense skin network depositing by layers of cationic and anionic charges on the support which attracts various ion transports across these membranes. The porous supports are mostly asymmetric structure obtained by phase inversion technique where the casting homogenous solution is immersed in non-solvent bath. In this way, an exchange of solvent and non-solvent causes phase separation and forms membrane. However, the phase inversion method is complicated depending on thermodynamic properties of the raw materials and often encounters two major limitations which are relatively low porosity and poor pore-size distribution (Wang et al., 2006). Electrospinning is one of the techniques that can overcome some of these problems. In such process, the non-woven fiber, so called electrospun fiber, is generated in such a way that high porosity and large surface area are yielded. For desalination purpose, cellulose acetate (CA) was often used to produce membrane as it has high chlorine resistance.

In this work, composite membranes were generated with CA electrospun fiber as a support to replace the poor performance asymmetric porous structure, and coated by polycation/polyanion multilayers (potentially sodium alginate (SA), poly (styrene sulfonate) sodium salt (PSS), and chitosan (CHI). Permeation flux and ion selectivity of the membrane were examined along with the effect of the number of bilayers on the desalination performance.

1.2 Objectives

To study effects of surface modification with polyelectrolyte multilayers on desalination performance of the resulting membrane.

1.3 Scopes of this work

- The top layers of composite membranes were alternate polycation and polyanions as multilayer deposition.
- Polycation employed in this work included chitosan (CHI) whereas polyanions included sodium alginate (SA) and poly (styrene sulfonate) sodium salt (PSS).
- The number of bilayers was investigated for the fabrication of composite membranes.
- Effects of the NaCl concentrations were studied for desalination performance of composite membrane.

CHAPTER II

BACKGROUNDS & LITERATURE REVIEW

2.1 Membrane technology

Membrane technology is important for separation, purification and increasing concentration as it works without the addition of chemicals, and with a relatively low energy requirement. The main principle of membrane processes is to have some kinds of driving force such as concentration gradient and pressure for the solution to pass through the membrane. Typically, membrane acts as intermediate between the two phases and the separation efficiency depends on the permeability towards the target compounds of the membrane. Process separation is classified as shown in Figure 2.1 which indicates that reverse osmosis and nanofiltration processes can be employed for desalination purposes.

size (um)							
	0.001	0.01	0.1	1	10	100	1000
appox. molecular wt.							
	100	200 1000 10000 20000	100000	500000			
molecule/particle	aqueous salts / ion / sugar	pyrogen / virus / colloidal / protien albumin	carbon black / tobacco smoke	pigment	yest cells / bacteria / dust / starch	fog	
process	reverse osmosis / nanofiltration	ultrafiltration	microfiltration		particle filtration		
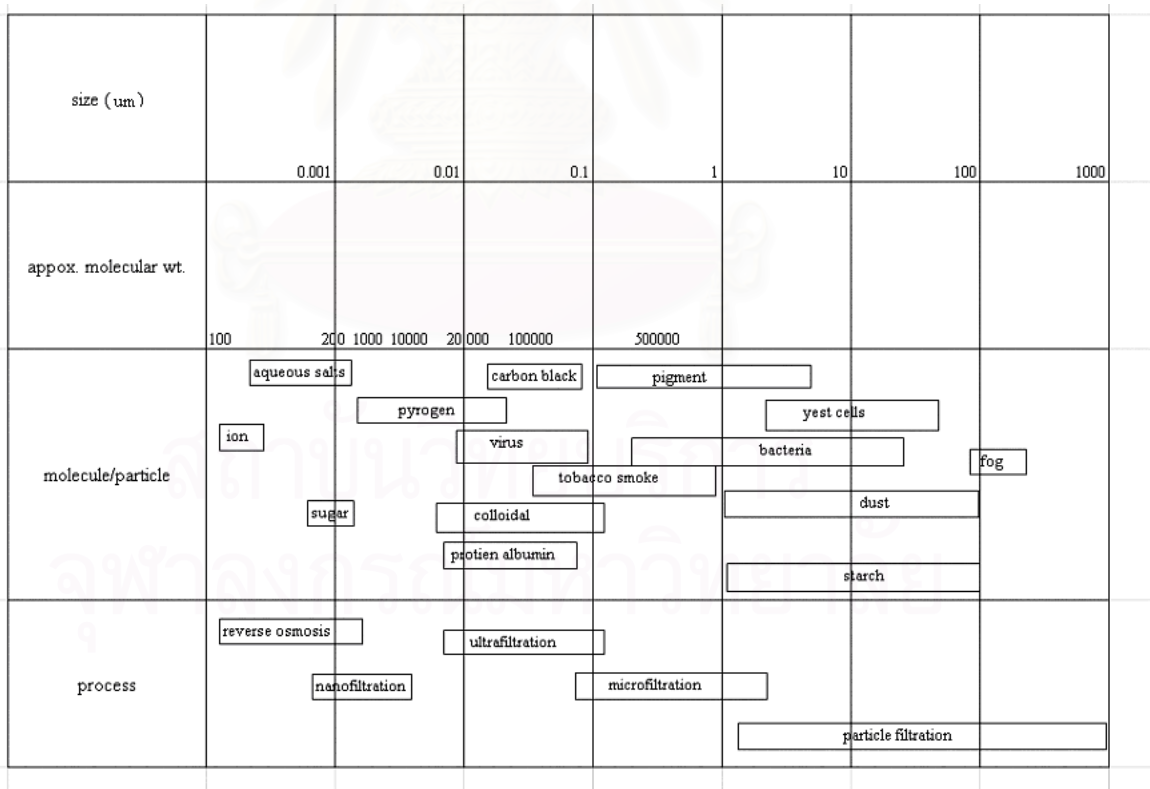
Figure 2.1 Schematic diagram of process separation (Jiraruttananont, 1998)

2.2 Reverse osmosis and nanofiltration processes

Reverse osmosis (RO) and nanofiltration (NF) processes are similar in that they can separate very small molecular contaminants, in the range compatible with the size of solvent. Generally, the performance for desalination of RO is better than that of NF. RO is typically used to separate salt ions while NF for the separation of multivalents but low monovalent ions. Thus, NF process is used for applications such as water softening and brackish water while RO process is suitable for the purification of seawater. Table 2.1 shows the difference between these processes.

Table 2.1 Characteristics of RO and NF processes (Jiraruttananont, 1998)

Characteristics	Reverse osmosis	Nanofiltration
mechanism	solution-diffusion	pore-flow solution-diffusion
driving force	pressure	pressure
operating pressure (bar)	20-40 for brackish water 40-80 for seawater	10-20
membrane structure	dense-asymmetric and skin layer or composite	dense-asymmetric mostly as composite
rejection		
monovalent ions (Na^+, K^+, Cl^-)	98-99.5%	40-90%
divalent ions (Ca^{2+}, Mg^{2+}, SO^{2-}_4)	>99%	>90%
bacteria, virus	>99%	>99%
MWCO 100-200	>90%	>50%
MWCO 200-500	>95%	>98%

In principle, RO membranes are freely permeable to water, but much less permeable to salt. This membrane property allows separation of salt from water where only water molecule passes through the membrane from the pure water side of the membrane into the salt side as shown in Figure 2.2(a). This process is called normal osmosis. If a hydrostatic pressure is applied to the salt side of the membrane, the flow of water can be retarded and, when the applied pressure is sufficient, the flow ceases (Figure 2.2b). The hydrostatic pressure required to stop the water flow is called the

osmotic pressure ($\Delta\pi$). If pressures greater than the osmotic pressure are applied to the salt side of the membrane, the flow of water is reversed, and water begins to flow from the salt solution to the pure water side of the membrane (Figure 2.2c). This process is called reverse osmosis (RO).

(a)   (b)   (c)
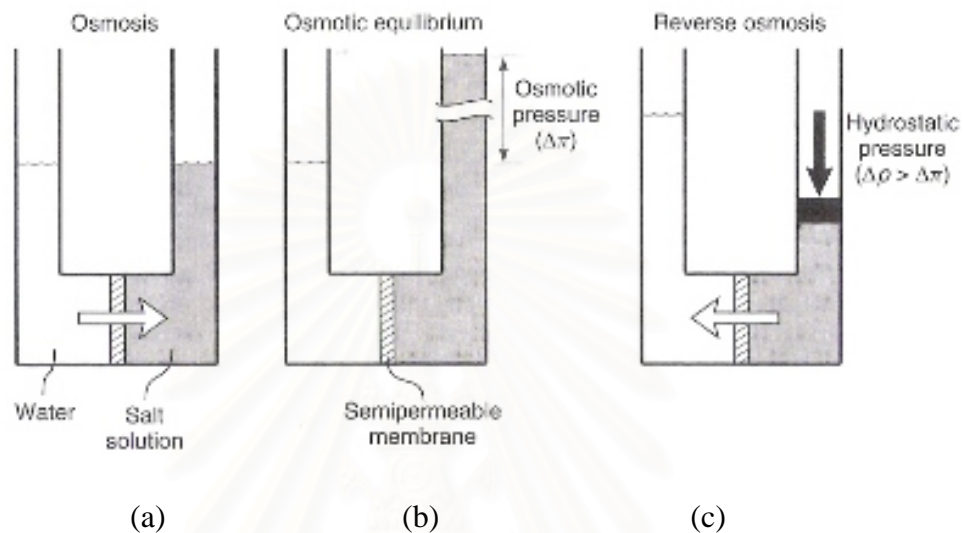
Figure 2.2 Schematic diagrams of (a) osmosis, (b) osmotic equilibrium and (c) reverse osmosis (Baker, 2004)

2.3 Theory

2.3.1 Transport mechanism

The most important property of membranes is their ability to control the rate of permeation of different species. The two models used to describe the mechanism of permeation are illustrated in Figure 2.3. The first one is the solution-diffusion model. In this model, the permeate dissolves in the membrane material and then diffuses through the membrane down a concentration gradient (Figure 2.3a). The permeate is separated because of the differences in the solubilities of the materials in the membrane and the differences in the rates at which the materials diffuse through the membrane. The other model is pore-flow model in which permeate are transported by pressure-driven convective flow through tiny pores (Figure 2.3b). Separation occurs because one of the permeate is excluded from some of the pores in the membrane through which other permeates move.

(a) (b)

Figure 2.3 Schematic of molecular transport through membrane: (a) molecular diffusion and (b) molecular filtration (Baker, 2004; Suntarapha, 2004)

For RO process, the transport solution is according to solution-diffusion model. The water flux is dependent on pressure and concentration gradients across the membrane following Equation 2.1:

$$J_w = \frac{\rho_w}{L_m}(\Delta P - \Delta \pi)$$
$$= A_w(\Delta P - \Delta \pi)$$

(2.1)

where J_w is the water flux, ρ_w permeability, L_m the membrane thickness, A_w solvent permeability constant, ΔP the pressure difference across the membrane and $\Delta \pi$ the difference osmotic pressure across the membrane. If applied pressure is lower than osmotic pressure ($\Delta P < \Delta \pi$), normal osmosis takes place and water transfers from dilute to concentrate salt sides. When applied pressure is equal to osmotic pressure ($\Delta P = \Delta \pi$), no flow occurs and when applied pressure is higher than osmotic pressure ($\Delta P > \Delta \pi$) , water flows from the concentrated to the dilute salt solution side the membrane.

The solute or salt flux depends on the concentration gradient driving force following Equation 2.2:

$$J_s = \frac{D_s K_s}{L_m}(C_f - C_p)$$
$$= A_s(C_f - C_p)$$

(2.2)

where J_s is solute flux, D_s diffusivity of solute in the membrane, K_s distribution coefficient, A_s solute permeability constant, C_f solute concentration in feed and C_p solute concentration in permeate.

Salt rejection is calculated from the indicated performance of the membrane, defined as

$$R = [1 - \frac{C_p}{C_f}] \times 100\% \qquad (2.3)$$

2.3.2 Modes of filtration

- Dead-end filtration

In dead-end filtration, the feed solution is flown perpendicularly with membrane (Figure 2.4a). After a sufficiently long operation time, the surface of membrane becomes accumulated with particles which are generally called cake. The accumulation of cake will increase flow resistance and rapidly decrease flux. Therefore the dead-end filtration should only be restricted to the use for cases with small particles and low concentration.
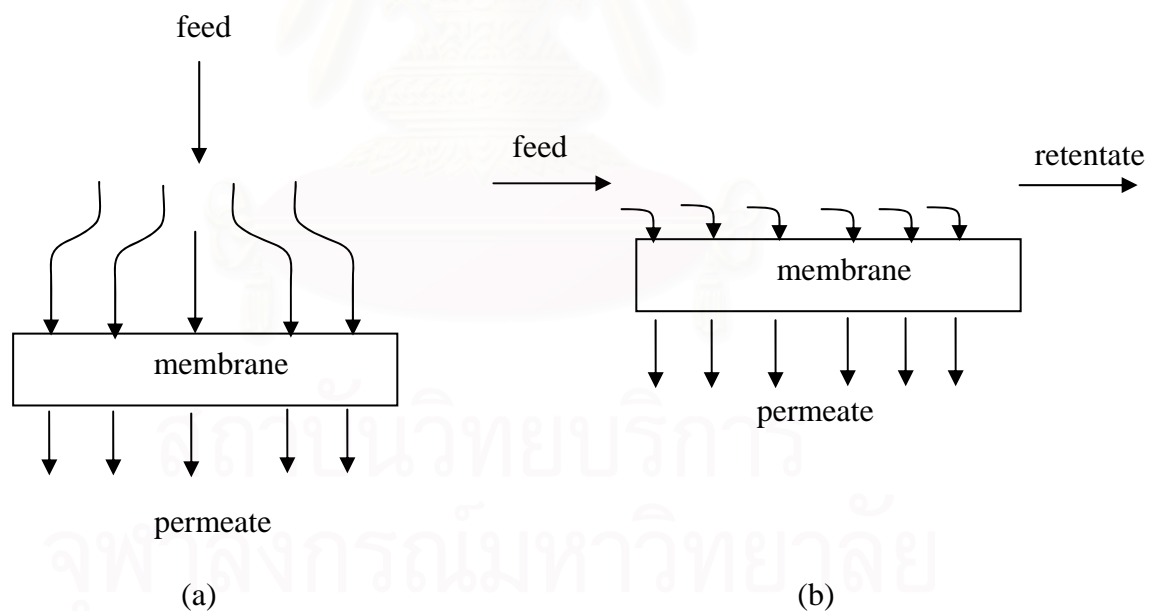
Figure 2.4 Schematic diagrams of modes of filtration: (a) dead-end and (b) cross-flow filtration

- Cross-flow filtration

In this case, the feed solution flow is parallel to the membrane (Figure 2.4b). The shear stress caused by the flow assists the reduction of the deposition of cake on the membrane surface. Hence, the water flux remains relatively constant independent of operation time, which is not the case with dead-end filtration. The cross-flow filtration mode is commonly used in process separation and suitable for high concentration solution. Summary of advantages and disadvantages of these filtration modes is given in Table 2.2.

Table 2.2 Advantages and disadvantages of dead-end and cross-flow filtrations

Mode of filtration	Advantages	Disadvantages
dead-end	- lower energy consumption	- lower flux for long time
	- suitable for small particle	- higher fouling on surface
	filtration	of membrane
		- usually cleaning
cross-flow	- higher flux for long time	- higher energy consumption
	- lower fouling	

2.4 Membrane types for RO and NF processes

- Nonporous, Dense Membranes

Nonporous, dense membranes shown in Figure 2.5 (a) consist of a dense film through which permeates are transported by diffusion under the driving force of pressure, concentration, or electrical potential gradient. The separation of various components of a mixture is related directly to their relative transport rate within the membrane, which is determined by their diffusivity and solubility in the membrane material.

<center>(a)   (b)</center>
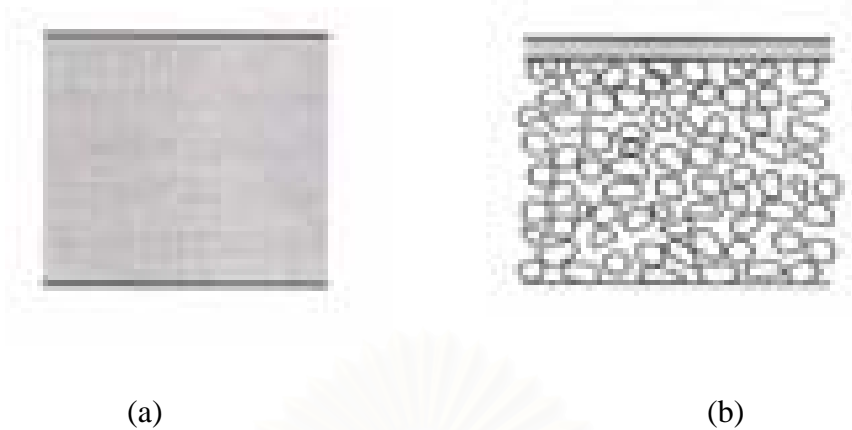
Figure 2.5 Schematic diagram of type membrane: (a) nonporous dense membrane, and (b) thin-film composite anisotropic membrane (Baker, 2004)

- **Composite membranes**

Desalination process requires very small pore size to dense membrane for ion separation. This has to be achieved through the use of composite membranes which typically consist of thin surface layers and porous support layers as illustrated in Figure 2.5 (b). The fabrication of the membrane layers is usually made from different polymers. These thin membranes are often fabricated on the surface of the porous support layers which are normally asymmetric (anisotropic) porous membranes of which porosity and pore-size change from top to bottom of the membrane. These porous layers are mostly prepared by the phase inversion method. The separation properties and permeation rates of the membrane are determined exclusively by the surface layer. The advantages of the higher fluxes provided by anisotropic membranes are so great that almost all commercial processes use such membranes.

2.5 Polymeric membrane preparations for desalination
2.5.1 Nonporous (dense) membranes

Nonporous (dense) membranes are rarely used in membrane separation because flux inverse proportional to thickness. The membrane is prepared by solution casting or thermal melt processing. Solution casting is commonly used to prepare small samples of membrane for characterization. Polymer solution used for solution casting should be sufficiently viscous to prevent it from running over the casting plate

and solvents are moderately volatile. The polymer solution is spread on flat plate. After casting, the solution is left to stand and the solvent evaporates to leave a thin polymer film. The other process is thermal melt processing as melt extruded film suitable for many polymers do not dissolve in solvent at room temperature such as polyethylene, polypropylene and nylons. The polymers are heated to melting point and extruded as sheet film.

2.5.2 Anisotropic (asymmetric) porous membranes

Anisotropic membranes are layers structures in which the porosity, pore-size or even membrane composition change from the top to the bottom surface of the membrane. Mostly, methods for preparing membrane are phase inversion and interfacial polymerization.

- **Phase inversion method**, phase inversion is homogenous polymer solution which changes to heterogeneous solution and to gel. During the phase change, skin layer and porosity in film or gel were obtained. The polymer solution mostly consists of three main components; polymer, solvent and non-solvent. The polymer solution or what is called sol 1 (Figure 2.6a) is casted on glass plate where a part of solvent evaporates and at this point, phase separation and gel occurs and the solution is called Sol 2 (Figure 2.6b). Polymer chains move assembly similar to micelles and when solvent decreases, micelles move more closely (Figure 2.6c). When this film is immersed in non-solvent (water) coagulation bath, solvent from film transfers through water and film solidifies. At the same time, some water moves through to the film. The micelles are in contact with each other (Figure 2.6d) and the exchange of polymer occurs. The micelles will form a network (Figure 2.6e) and begins to shrink as pores occur (Figure 2.6f) due to the solidification. If the walls of micelles are thin, walls tear apart giving more open porous structure in membrane. In contrast, if the walls have high thickness, tear of the wall is difficult so small pores are resulted. The diagram of porous mechanism is shown in Figure 2.6.
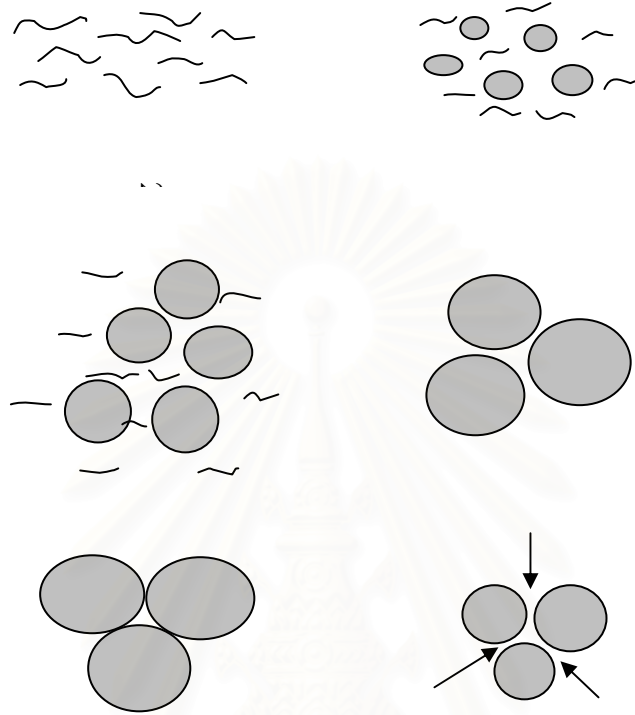
Figure 2.6 The diagram of porous mechanism: (a) homogenous polymer solution
(Sol 1), (b) heterogeneous polymer solution and micelles occur (Sol 2), (c) the
micelles move more closely , (d) the micelles contact with each other, (e) net work
structure of micelles, and (f) the walls of micelles shrink to porous

- **Interfacial polymerization** is the method used to improve salt rejection and
water flux but not resistance to chlorine. Most reverse osmosis membranes are made
by this method. Schematic of the interfacial polymerization process is shown in
Figure 2.7 where an aqueous solution of a reactive prepolymer such as polyamine is
first deposited in the pores of a microporous support membrane, typically a
polysulfone ultrafiltration membrane. The amine-loaded support is then immersed in a
water- immiscible solvent solution containing a reactant such as a diacid chloride in
hexane. The amine and acid chloride react at the interface of the two immiscible
solutions to form a densely crosslinked. For example, Roh et al. (2006) prepared thin

film composite (TFC) membrane from m-phenylenediamine and trimesoyl chloride reaction on polysulfone support for NaCl separation where the water flux was 23 L/m^2h and salt rejection was about 98% which were relatively high when compared with typical values of 17 L/m^2 h and 91 %, respectively (see Tables 2.3 and 2.4 for details).
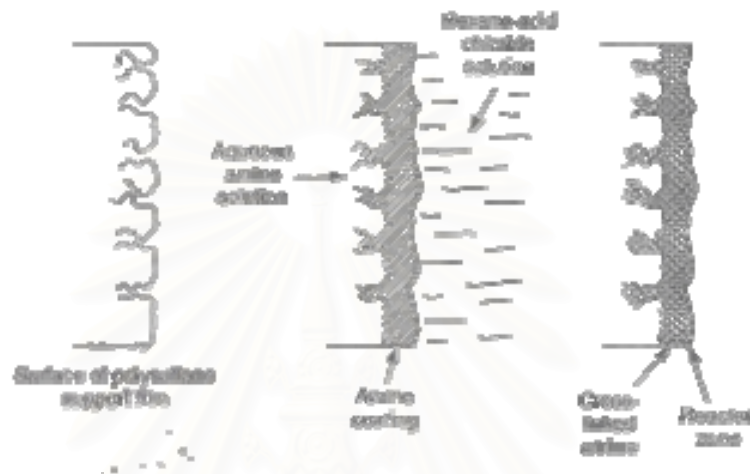
Figure 2.7 Schematic of the interfacial polymerization process (Baker, 2004)

2.6   Electrospinning technique

Electrospinning is a process of electrostatic fiber formation which uses electrical forces to produce polymer fibers from polymer solution or so called nanofibers or ultrafine fibers or electrospun fibers in a form of non-woven fibers. Ultrafine fibers have diameters in the range from sub-micrometer down to nanometer. The ultrafine fibers have many benefits such as a large specific surface area, high porosity and ease of fabrication. It is potentially applicable to several processes such as filtration, tissue engineering, wound dressing and others.

A schematic diagram of electrospinning process is demonstrated in Figure 2.8. It consists of the syringe containing polymer solution, the metallic collector and the high voltage power supply.

High electric field strength is generated between a polymer solution and a metallic collector. The hemispherical shape of pendant droplet at the end of syringe tip is changed into a conical shape with increasing voltage that is called Taylor cone. When the voltage reaches a critical value at which the electric forces overcome the surface tension, a charged jet of the solution is ejected from the tip of a cone

protruding from a liquid drop of the polymer. As the jet undergoes a bending instabilities, stretches, elongates and the solvent evaporates in the air. The non-woven fibers are obtained on collector.
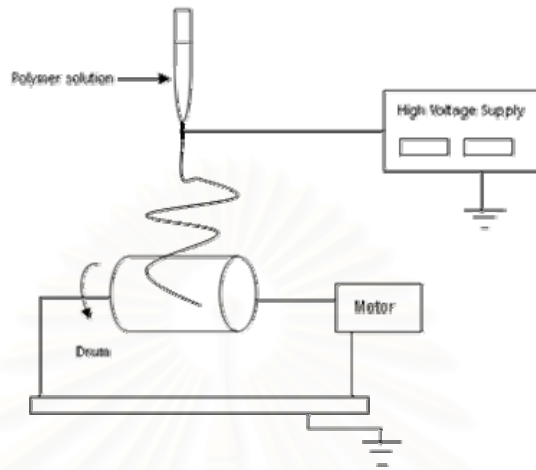
Figure 2.8 Electrospinning process

There are six major forces acting on an infinitesimal segment of the charged jet.
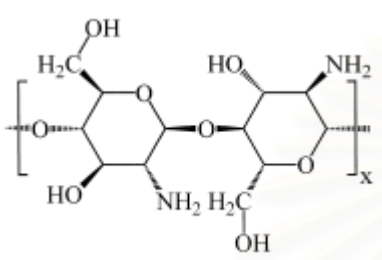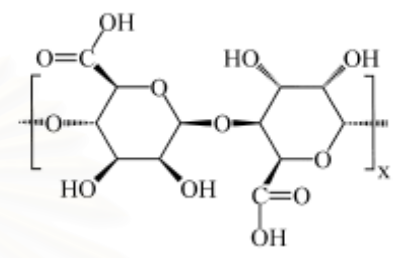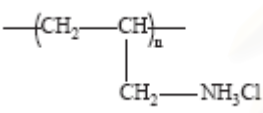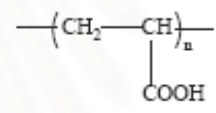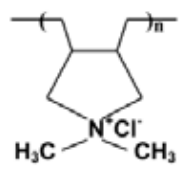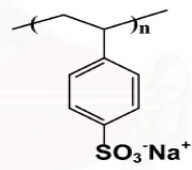
1. Body or gravitational forces.
2. Electrostatic forces which carry the charged jet from the nozzle to the target.
3. Coulombic repulsion forces which try to push apart adjacent charged species present within the jet segment and are responsible for the stretching of the charged jet during its flight to the target.
4. Viscoelastic forces which try to prevent the charged jet from being stretched.
5. Surface tension which also acts against the stretching of the surface of the charged jet.
6. Drag forces from the friction between the charged jet and the surrounding air.

2.7 Electrostatic self-assembly layer-by-layer coating

The top layer of the composite membrane is prepared by coating with layer-by-layer deposition of cationic and anionic polyelectrolytes. This technique is simple, cost effective and environmentally friendly. The porous support is immersed into solution containing polyanion and polycation, between which the membrane is rinsed with water. The properties of multilayer film are variable depending on polyelectrolyte structure, the number of deposited layers, pH and ionic strength of

deposition solutions. Several literatures reported different types of polyelectrolytes used as composite membranes as illustrated in Table 2.3.

Table 2.3 Example of types of polyelectrolyte used for multilayer deposition

polycationic	polyanionic
chitosan = CHI	sodium alginate = SA

poly(allylamine hydrochloride) = PAH	poly(acrylic acid) = PAA

poly(diallyldimethylammonium chloride) = PDADMAC	poly(sturene sulfonate) sodium salt = PSS

polyvinylamine = PVA	polyvinylsulphate (potassium salt) = PVS

$-(CH_2\text{-}CH_2\text{-}NH\text{-})_n$

$-(CH_2\text{-}CH\text{-})n$

$$SO_3^-\ K^+$$

2.8 Polymeric materials for composite membrane in this work

Desalination process requires membrane to be stable over a wide range of pH, temperature and good mechanical durability. Different types of materials have been employed for the fabrication of composite membranes and some of them are mentioned below.

- **Cellulose acetate**

Cellulose acetate (CA) whose chemical structure is illustrated in Figure 2.9 is a hydrophilic polymer but water insoluble, environmentally friendly and especially chlorine tolerance which makes it attractive as membrane for desalination. The cellulose acetate membranes can be relatively easy to make, mechanical tough, and resistant to degradation by chlorine (up to 1 ppm) and other oxidants. The flux and rejection depend on many parameters such as polymer dope concentration, thickness of membrane and degree of acetylation. For example, Haddad et al., 2004 prepared nanofiltration cellulose acetate membrane by the phase inversion method for brackish water desalination. The resulting demonstrated high water flux and salt rejection are 7.18 L/m^2 h and 86% respectively for higher polymer concentration.
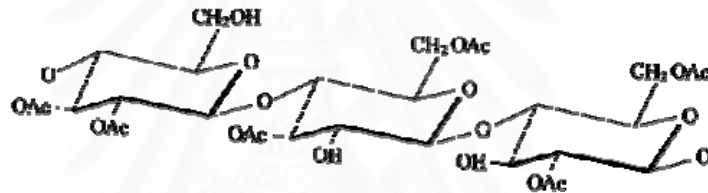
Figure 2.9 Cellulose acetate structure (Ac = -COCH$_3$)

CA membrane can be easily produced by electrospinning technique and the resulting membrane has relatively high porosity of about 85% (Ma et al., 2005) and large surface area. When the CA membrane is used as support of polyelectrolyte skin layers, it is treated with alkaline solution through hydrolysis reaction, and this converted the acetyl group to carboxylic group and increased the negative charge at the surface. Therefore an improve adhesion of polyion at surface layer could be obtained.

- **Chitosan**

Chitosan (CHI) consists of randomly distributed ß-(1-4)-linked D-glucosamine (deacetylated unit) and N-acetyl-D-glucosamine (acetylated unit) as shown in Figure 2.10. CHI is obtained by N-deacetylation of chitin which is a hydrophilic polysaccharide, non-toxic, odorless, water insoluble but water permeable. It is cationic polyelectrolyte that can bind to negatively charged substances.
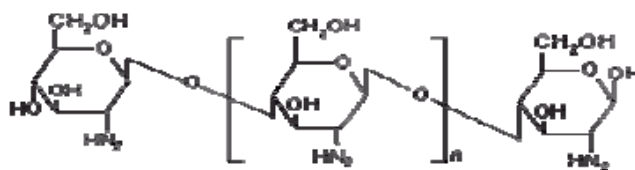
Figure 2.10 Chitosan structure

CHI has amine groups and when dissolved in acid solvent at optimum condition; amine group is protonated with proton demonstrating cationic charges. Thus CA is one of the potential choices of polycationic polymers for the fabrication of electrostatic self-assembly skin layer of composite membrane.

- **Sodium alginate**

Sodium alginate (SA) $(NaC_6H_7O_6)_n$ is an anionic polysaccharide obtained from the extraction of brown algae. SA is a linear copolymer of β-D-Mannuronic acid and α-L-Guluronic acid as illustrated in Figure 2.11. It is odorless, non-toxic, readily dissolved in water and insoluble in ethanol and ether. SA membranes are soluble in water, and so it is necessary to be crosslinked with crosslinking agents such as calcium chloride in order to improve water resistance (Yeom et al., 1998). The carboxyl groups of structure demonstrate negative charge and can be used as polyantionic agent to fabricate electrostatic self-assembly with polycationic as active skin layer of composite membrane.

(a)

(b)
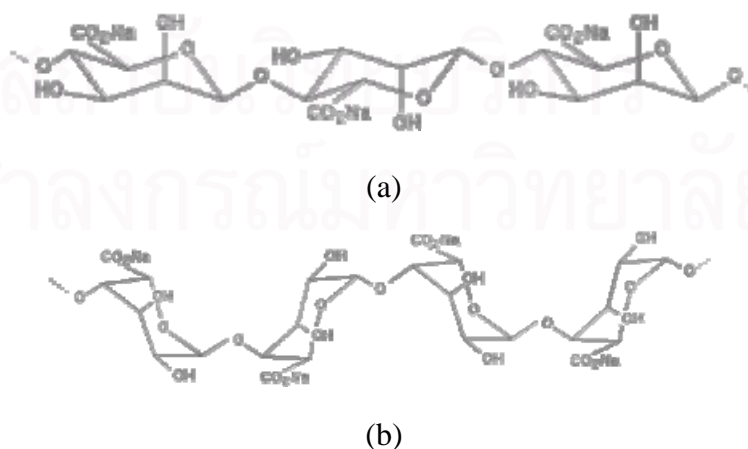
Figure 2.11 Sodium alginate structure (a) β-D-Mannuronic acid and (b) α-L-Guluronic acid

- **Poly (styrene sulfonate) sodium salt**

Poly (styrene sulfonate) sodium salt (PSS) is prepared by polymerization of styrene and then treating with sulfur trioxide as polystyrene sulfonic acid. The acid is neutralized using sodium hydroxide and the resultant product is obtained (Figure 2.12). The PSS is anionic polyelectrolyte with highly charged surface due to the presence of sulfonic group as substitution of aromatic rings on the polymer backbone. The benefits of this polymer are stable in broad pH range and good complex build up with cationic.

| Polystyrene | Polystyrene sulfonic acid | Poly (styrene sulfonate) |
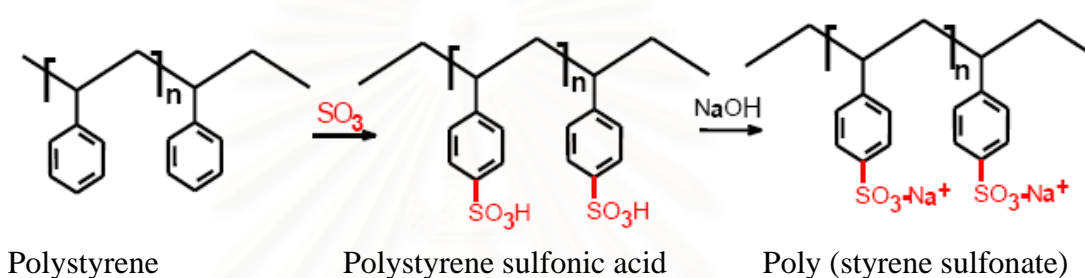
Figure 2.12 Reaction of poly (styrene sulfonate) sodium salt

2.9 Remarks on literature reviews: Desalination membranes

Polymeric materials have been generally reported as membrane for desalination. Due to its chlorine resistance properties, cellulose acetate (CA) is commonly employed for this purpose (Jiraruttananont, 1998; Ferjani et al., 2002; Baker, 2004; Suntarapha, 2004). CA is hydrophilic polymer forming asymmetric polymeric membranes when underwent the preparation through the phase inversion method (Ferjani et al., 2002; Haddad et al., 2004; Lajimi et al., 2004). The efficiency of CA membrane was in the range from ultrafiltration to reverse osmosis systems depending significantly on the membrane pore size which was controlled by several parameters such as polymer concentration and annealing temperature (Haddad et al., 2004; Ferjani et al., 2004). In general, salt rejection increased with an increase in polymer concentration and annealing temperature which reduced the pore size of the membrane (Haddad et al., 2004). For desalination, salt rejection could be up to 80%, and this could be enhanced further by the addition of hydrophobic polymers such as polymethylhydrosiloxane (PMHS) blended with CA solution or coated on CA support as composite (Ferjani et al., 2002; Ferjani et al., 2004). However, the enhanced salt rejection often was counterbalanced by a decrease in permeation flux (Ferjani et al.,

2002). Literature reviews on the use of CA and the modification of CA for certain purposes are shown in Table 2.4.

Several literature demonstrated polyelectrolyte multilayer membrane for desalination. The thin layer was obtained from two oppositely charged polyelectrolytes deposited on solid support. The numbers of polyelectrolyte bilayers are sufficient to cover pore of support and pH under optimum condition. The ion rejection in decreasing order was SO_4^{2-} >Cl^- (Hong et al., 2006) and $Mg^{2+} \geq Ca^{2+} >$ Na^+ (Stanton et al., 2003) for anions and cations, respectively. This strong rejection could be due to the high charged density of the divalent ions which possessed stronger repulsive force. Literature reviews on the performance of multilayer membranes are shown in Table 2.5.

Table 2.4 Literature reviews of cellulose acetate and modified membrane for desalination

Author, year	support	method	Top layer coating	anneal temperature of membranes	separation	Permeation flux (L/m²h)	Salt rejection	Mode of filtration (module)	Condition of filtration
Ferjani et al., 2002	(1) cellulose acetate 22 wt% (thickness ~250 μm)	phase inversion	-	79 °C	NaCl 2000 ppm	21	52 %	Dead-end (flat)	Pressure 15 bar Temperature 25 °C Effective area 38.5 cm²
	(2) cellulose acetate 22 wt% blend PMHS 2 wt%	phase inversion	-	79 °C	NaCl 2000 ppm	19	81%	Dead-end (flat)	Pressure 15 bar Temperature 25 °C Effective area 38.5 cm²
	(3) cellulose acetate 22 wt%	phase inversion	PMHS 20 wt% (thickness ~12 μm)	79 °C	NaCl 2000 ppm	17	91%	Dead-end (flat)	Pressure 15 bar Temperature 25 °C Effective area 38.5 cm²

Author, year	support	method	Top layer coating	anneal temperature of membranes	separation	Permeation flux (L/m²h)	Salt rejection	Mode of filtration (module)	condition of filtration
Haddad et al., 2004	cellulose acetate 22 wt% (thickness ~250 μm)	phase inversion	-	80°C	Brackish water TDS 3.9 g/L	(water) 7.2	86.12%	Dead-end (flat)	Pressure 16 bar Temperature 25 °C Effective area 38.5 cm²
Ferjani et al., 2004	cellulose acetate 22 wt% (thickness ~250 μm)	phase inversion	PMHS 20 wt%	80°C	brackish water TDS 4100g/m³	5.8	90%	Dead-end (flat)	Pressure 1.6 MPa Temperature 25 °C Effective area 38.5 cm²

polymethylhydrosiloxane = PMHS

Table2.5 Literature reviews of modified surface with multilayer deposition of polyelectrolytes for desalination

Author, year	support	anionic/cationic polyelectrolyte	number of polyelectrolyte bilayers	separation	Permeation flux (L/m^{2}h)	Salt rejection	Mode of filtration (module)	Condition of filtration
Stanton et al.,2003	porous alumina (0.02 μm)	PSS(pH2.1)/ PAH (pH2.3)	4.5	Na$^+$ 1000ppm	92	29%	cross-flow	pressure 4.8 bar effective area 1.5 cm^2 feed flow rate 18 mL/min
				SO$_4^{2-}$ 1000 ppm	67	56%		
				Ca^{2+} 1000 ppm	63	86%		
				Mg^{2+} 1000 ppm	50	96%		
Lajimi et al., 2004	cellulose acetate 20 wt%	CHI (pH5)/ SA (pH6)	25	MgSO$_4$ 0.017 M	results not shown	99%	dead-end (flat)	pressure 16 bar temperature 25 °C effective area 38.5 cm^2
				NaCl, 0.034 M	results not shown	75%		

Author, year	support	anionic/cationic polyelectrolyte	number of polyelectrolyte bilayers	separation	Permeation flux (L/m²h)	Salt rejection	Mode of filtration (module)	Condition of filtration
Toutianoush et al.,2005	polyacrylonitrile/ polyethylene terephthalate	PVA (pH1.7)/ PVS (pH1.7)	60	NaCl 10 mM	3.5	93%	dead-end (flat)	pressure 40 bar temperature 25 °C effective area 36.8 cm²
				MgCl₂ 10 mM	3.7	complete		
				Na₂SO₄ 10 mM	3.6	98.5%		
				MgSO₄ 10 mM	4	complete		
Hong et al., 2006	porous alumina (0.02 μm)	PAA (pH7.0)/ PAH (pH7.0)	4.5	SO₄²⁻ 1000 ppm	7	93%	cross-flow	pressure 4.8 x 10⁵Pa effective area 1.5 cm² feed flow rate 18 mL/min
				Cl⁻ 1000 ppm		13%		

Author, year	support	anionic/cationic polyelectrolyte	number of polyelectrolyte bilayers	separation	Permeation flux (L/m^2h)	Salt rejection	Mode of filtration (module)	Condition of filtration
		PAA(pH4.5)/ PDADMAC (pH4.5)	4.5	SO_4^{2-} 1000 ppm	58	24%	cross-flow	pressure $4.8 \times 10^5 Pa$ effective area $1.5 \, cm^2$ feed flow rate 18 mL/min
				Cl^- 1000 ppm		-4%		
		PSS(pH2.1)/ PAH (pH2.3)	4.5	SO_4^{2-} 1000 ppm	96	78%		
				Cl^- 1000 ppm		-9%		
		PSS (pH7.0)/ PDADMAC (pH7.0)	4.5	SO_4^{2-} 1000 ppm	100	92%		
				Cl^- 1000ppm		-16%		

Author, year	support	anionic/cationic polyelectrolyte	number of polyelectrolyte bilayers	separation	Permeation flux (L/m²h)	Salt rejection	Mode of filtration (module)	Condition of filtration
Hong et al., 2007	porous alumina (0.02 μm)	PSS (pH7.0)/ PDADMAC (pH7.0)	4.5	Cl⁻ 1mM	146	10%	cross-flow	pressure 4.8 bar effective area 1.5 cm² feed flow rate 18 mL/min
				F⁻ 1mM		73%		
		PSS(pH2.1)/ PAH (pH2.3)	4.5	Cl⁻ 1mM	196	16%		
				F⁻ 1mM		22%		

chitosan = CHI

poly(allylamine hydrochloride) = PAH

poly(diallyldimethylammonium chloride) = PDADMAC

polyvinylamine = PVA

sodium alginate = SA

pol(acrylic acid) = PAA

poly(sturene sulphonate) = PSS

polyvinylsulphate = PVS

CHAPTER III

MATERIALS &METHODS

3.1 Materials and chemical reagents

- Acetone (AR grade, 99.5%), VWR International Ltd
- Cellulose acetate ($M_w \sim 30,000$, 39.8 wt% acetyl content) (CA), aldrich
- Chitosan middle-viscous (M_w 400 kDa, degree of acetylation ~ 84.5%) (CHI), fluka
- Deionized water
- Glatial acetic acid 99.9%, J.T.Baker
- *N,N*-dimethyl acetamide (AR grade, 99%), (DMAc), Carlo Erbo
- Poly (styrene sulfonate) sodium salt (PSS) (M_w 70000, 30 wt% solution), aldrich
- Sodium alginate (by GPC M_w ~700,000) (SA), fluka
- Sodium chloride (NaCl, 99.9%), APS Chemical limited

3.2 Equipments

- BET (Micromeritics ASAP 2010)
- Conductivity meter (Suntex Conductivity meter SC-170)
- 47 mm Filtration Assemblies, Wheaton
- Fourier Transform Infrared Spectroscopy (FTIR) (Thermo Nicolet Nexus 670)
- Glass syringe
- High voltage power supply (Protek DC power supply DF 1730SB3A)
- Metal collector
- Scanning Electron Microscope (SEM) (JSM 5410 LV)
- Thermogravimetric analysis (TGA) (Diamond Thermogravimetric / Differential Thermal Analyser, PerkinElmer^{Tm})
- Vacuum pump (PHYWE 02750.93, Germany)
- X-ray photoelectron spectroscopy (XPS) (Kratos Amicus)

3.3 Procedure

3.3.1 Electrospinning of electrospun CA fibrous membranes

1. Prepare CA solution at a fixed concentration of 16 % weight by volume (Tungprapa et al., 2007) by dissolving 1.92 g CA powder in a solvent mixture between acetone (8 mL) and DMAc (4 mL) (volume ratio of acetone to DMAc equal 2:1), stir at room temperature until homogenous solution

2. Fill CA solution in the glass syringe

3. Apply 12 kV voltages and rotate the metal drum collector at a speed of about 100 rpm, keep the distance between metal drum collector and the nozzle at 15 cm. See a schematic in Figure 3.1

4. Store sample in desiccator for 24 h

5. Peel electrospun CA fibrous membranes from metal collector
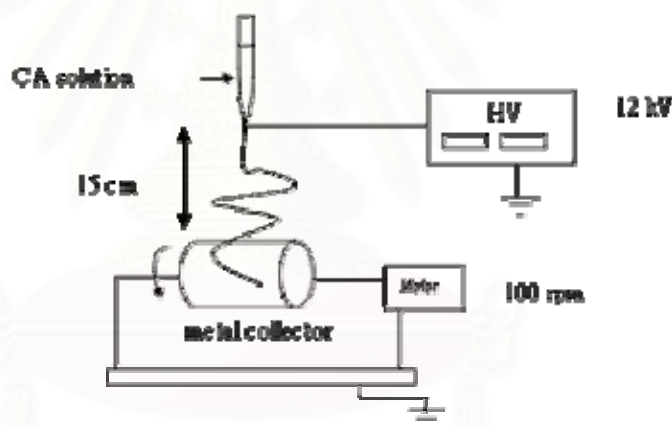
Figure 3.1 Setup of electrospinning set

3.3.2 Preparation polelectrolyte multilayer composite membranes

1. Prepare CHI cationic solution at a fixed concentration 0.4 % weight by volume (Park et al., 2007) by dissolving 4 g CHI in acetic acid solution 1% volume by volume (1000 mL)

2. Prepare SA anionic solution at a fixed concentration 1 % weight by volume (Park et al., 2007) by dissolving 10 g SA in deionized water (1000 mL)

3. Immerse the specimens of the base electrospun CA fibrous membranes in CHI and SA solutions for about 5 min, rinse in deionized water between each layer for about 2 min

4. Repeat sequence of number of bilayers in the range of 15-25 bilayers

5. Prepare PSS anionic solution in deionized water at a concentration 0.4 %weight by volume (Haack et al., 2001) (1000 mL)

6. Replace SA by PSS and repeat Steps 3 to 4

7. Dry composite membrane at $60^{o}C$ for 12 h

(The physical properties of polyelectrolyte solution is report in the appendix)

3.4 Characterization

3.4.1 Scanning Electron Microscope (SEM)

Characterize surface morphology of both the base and the coated electrospun CA fibrous membranes and measure fiber diameter (90 fibers) and pore size on surface by Semafore®5 program

*Remark: the pore size was measured from the circle that could fit right in the space between fibers

3.4.2 Horizontal Attenuated Total Reflectance Fourier Transform Infrared Spectroscopy (HATR-FTIR)

Observe the functionalities of both the base and the coated electrospun CA fibrous membranes over a wave number range of 400-4,000 cm^{-1}

3.4.3 X-ray photoelectron spectroscopy (XPS)

Investigate elements on surface membrane with Mo Kα source for excitation at 10 mA and 20 kV

3.4.4 BET analysis

Measure surface area of samples by the BET nitrogen adsorption at 77 K, degassed at $120^{o}C$

3.4.5 Thermal property

Measure the thermal property by thermogravimetric analysis (TGA) at a heating rate of $10^{o}C/min$ under N_2 atmosphere from 50 to $550^{o}C$

3.4.6 Water permeability

1. Put the coated electrospun CA fibrous membranes on the propylene support (commercial, Pall Life Science) and set dead-end filtration test, 47 mm Filtration Assemblies at room temperature and inlet pressure at atmospheric pressure and outlet pressure at vacuum pressure (See schematic in Figure 3.2).

2. Determine permeation flux of water following equation (3.1) following condition:

> Volume of the testing solution = 50 mL
>
> Effective area of the tested membrane = 9.6 cm^2
>
> Sampling time = 10 min
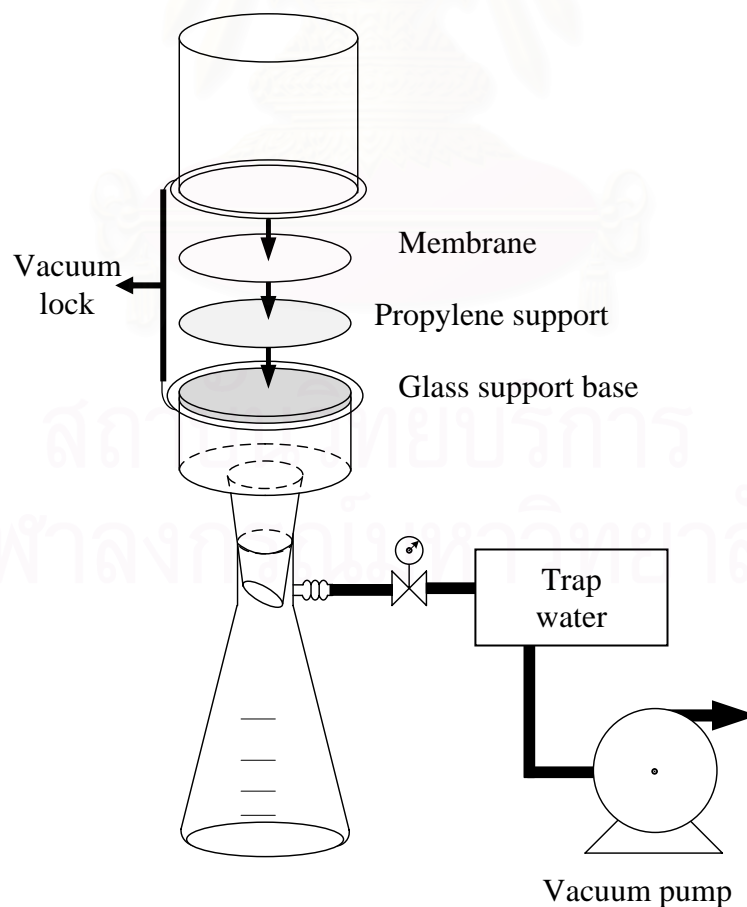
Figure 3.2 Schematic of separation test

3.4.7 NaCl solution rejection test

1. Prepare aqueous NaCl solution in the concentration range of 1,000 – 3,000 ppm

2. Set sample and apparatus test as detailed in the water permeability test (Section 3.4.5)

3. Determine permeation flux of solution with Eq. 3.1 and salt rejection with Eq. 3.2, following condition:

    Volume of the testing solution = 100 mL

    Effective area of the tested membrane = 9.6 cm^2

    Sampling time = the time when the volume of permeate at 50 mL

3.4.8 Calculations

1. Permeation flux is calculated from the following equation

$$J = \frac{Q}{A\Delta t} \tag{3.1}$$

where J is the permeation flux (L m^{-2} h^{-1}), Q is the permeation volume of the testing solution, A is the effective area of the tested membrane (m^2) and Δt is the sampling time (h).

2. Salt rejection is calculated from the following equation

$$R = [1 - \frac{C_p}{C_f}] \times 100\% \tag{3.2}$$

where C_f and C_p represent the salt concentration of the feed and the permeate solution which are determined by conductivity measurements

CHAPTER IV
RESULTS & DISCUSSION

The composite membranes were characterized for their morphology by scanning electron microscope (SEM), functional groups by horizontal attenuated total reflectance fourier transformed infrared spectroscopy (HATR-FTIR), x-ray photoelectron spectroscopy (XPS) and thermal property by TGA analysis. The final membrane was tested in the desalination application.

4.1 The support of composite membranes

The base electrospun CA fibrous membrane was used as a support for the fabrication of composite membranes. This CA membrane was made electrospinning the 16 %weight by volume of CA solution in solvent mixture between acetone and dimethylacetamide (at 2:1 by volume). Fabricating conditions for this membrane are given in Chapter 3. The SEM image for this support CA membrane is shown in Figure 4.1 which illustrated a non-woven fiber structure with a fiber diameter of about 280 ± 38 nm. The average of the CA support membrane was about 110 µm.

.
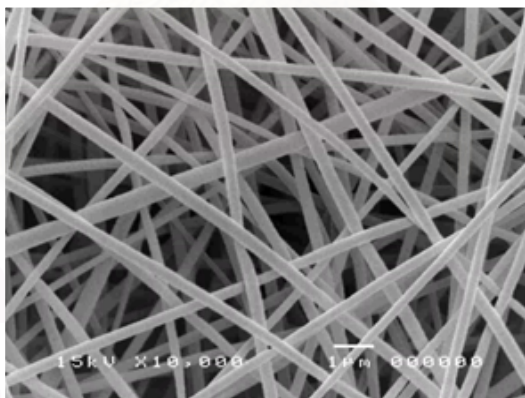
Figure 4.1 SEM image of base electrospun CA fibrous membrane

4.2 Characterization of composite membranes

4.2.1 Scanning Electron Microscope: SEM

The base electrospun CA fibrous membranes were successfully coated with polycation/polyanion multilayer as composite membrane composite using the method as described in section 3.3.2. The polycationic electrolyte employed in this work was chitosan (CHI) whereas the polyanionic electrolytes were sodium alginate (SA) and poly (styrene sulfonate) sodium salt (PSS). These polyelectrolyte layers may be considered to have physical network structure with ionic crosslinking of the oppositely charged ions from the cationic/anionic polyelectrolytes. The first layer of the composite membrane was selected as CHI layer as its amino groups represented positive charges which could be deposited more stably with the negatively charged hydroxyl group of electrospun CA fiber. The second layer was therefore the oppositely charged SA layer. After coated with polyelectrolytes (CHI/SA), the SEM image in Figure 4.2 (b-d) indicated that the pores at surface were no longer apparent when compared with the base electrospun CA fiber (Figure 4.2 (a)). In this figure, the subscript n in (CHI/SA)$_n$, i.e. 15, 20, and 25, indicated the number of bilayers coated on the electrospun membrane.

SEM images of the membrane products at various bilayers as shown in Figure 4.2 demonstrate that there were no significant differences among all samples. This may be because the polyelectrolyte layers formed like a dense phase blanket on the top of the porous support layer.

(a)

(b)

(c)

(d)
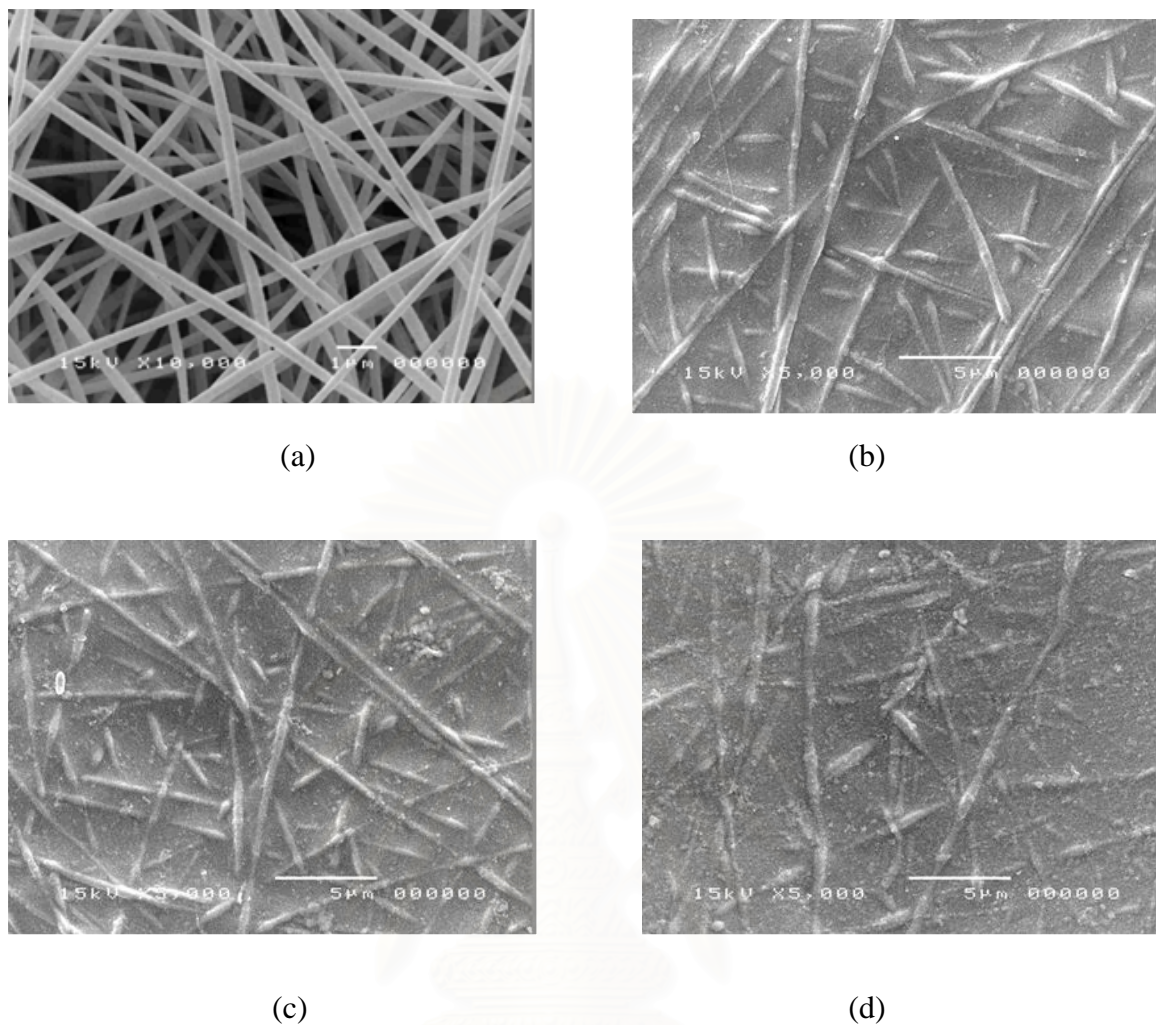
Figure 4.2 SEM images of (a) base eletrospun CA fibrous membrane, (b) (CHI/SA)$_{15}$ bilayers, (c) (CHI/SA)$_{20}$ bilayers, and (d) (CHI/SA)$_{25}$ bilayers

Alternative experiment was performed with SA replaced by PSS. The morphologies of membranes are shown in Figure 4.3. In this case, the surface of membranes was rough with a large number of pores distributed all over the surface area. This occurred regardless of the number of bilayers and it is one of the main physical appearances which were different from the morphology of the CHI/SA coated membrane where no such pores were apparent.

Table 4.1 summarizes morphology of the two different polyanionic polyelectrolyte membranes at 20 bilayers.

(a)

(b)

(c)

(d)
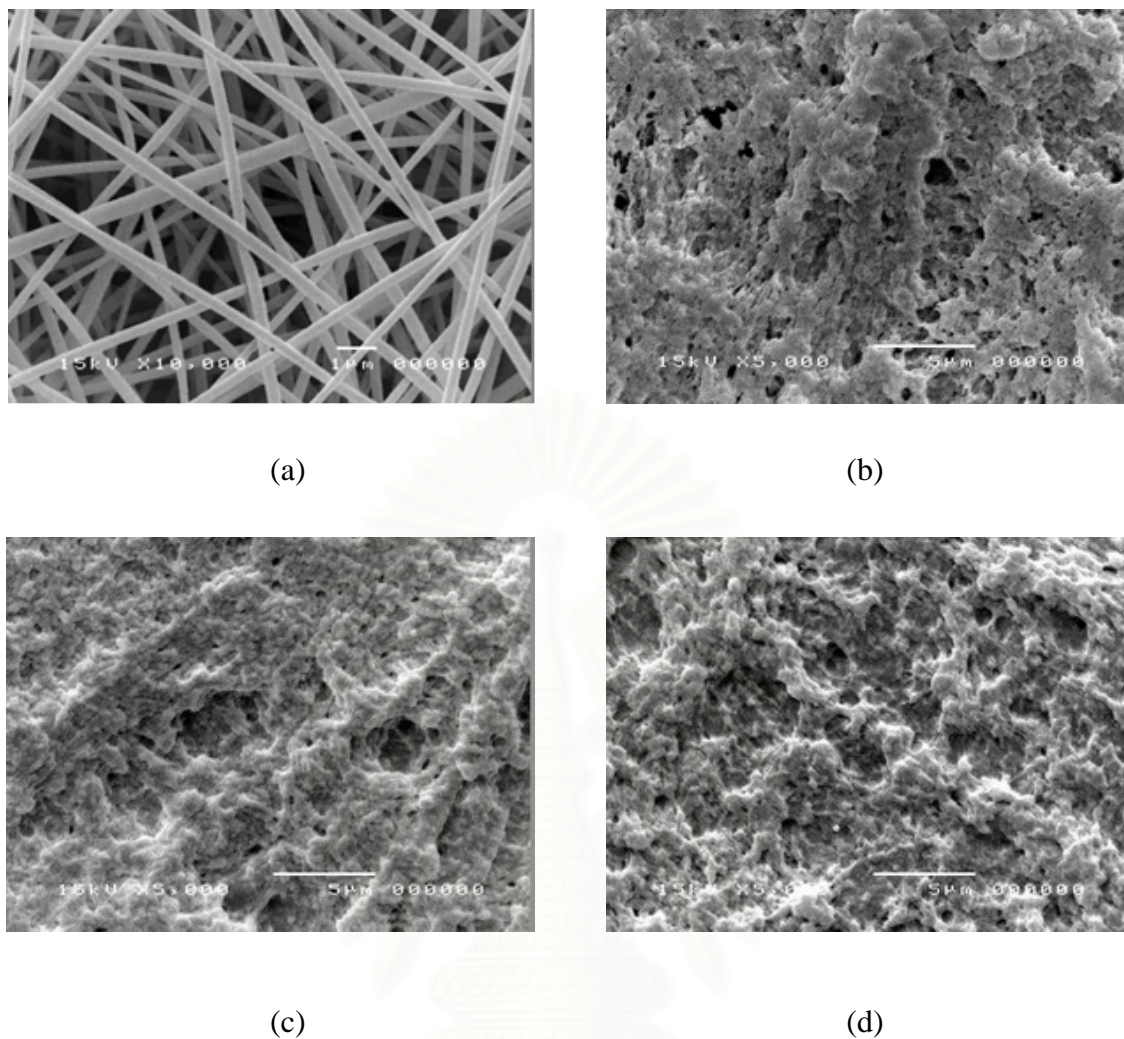
Figure 4.3 SEM images of (a) base eletrospun CA fibrous membrane, (b) (CHI/PSS)$_{15}$ bilayers, (c) (CHI/PSS)$_{20}$ bilayers, and (d) (CHI/PSS)$_{25}$ bilayers

Table 4.1 Summary of the different morphology of polyanionic polyelectrolytes at 20 bilayers

Characteristic	CHI/SA coated membrane	CHI/PSS coated membrane
Polyelectrolyte layer	smooth	roughness
Top layer	more dense	less dense
Apparent membranes	shiny	rough

4.2.2 Functional groups by horizontal attenuated total reflectance-fourier transformed infrared spectroscopy: HATR-FTIR

Before discussing the functional groups of the membrane product, it was recommended to consult Table 4.2 for the matching between FTIR absorption band and the potential functional groups. Figure 4.4 shows HATR-FTIR spectra of the base membrane compared with the CHI/SA coated membrane. In this figure the HATR-FTIR spectra of the CHI/SA$_{15}$ was illustrated along with that of CHI/SA$_{15}$CHI which represented the membrane with 15 alternate layers of CHI and SA whereby the top layer was coated with CHI (instead of SA). The CA fibrous membrane exhibited a strong carbonyl (C=O) absorption peak at 1,747 cm^{-1} due to the acetyl groups in CA structure. After the deposition of polyelectrolytes layer, the influential functional group of polyelectrolyte were presented. When the top surface was SA ((CHI/SA)$_{15}$), the peaks of carboxyl salt of SA showed clear absorption band of carboxyl anion (COO$^-$) at 1,596 and 1,411 cm^{-1} (Figure 4.4 (b)). On the other hand, when the top layer was CHI, it was expected to observe clear peaks of amino groups ((CHI/SA)$_{15}$CHI) which constituted the main port in chitosan structure but these only existed as very weak peaks (Figure 4.4 (c)). This could be that the amino peaks such as the secondary amide at 1,515–1,570 cm^{-1} and the primary amine at 1580-1325 cm^{-1} (Wang et al., 2004) overlapped with the strong peak of carboxyl group.

Figure 4.5 shows HATR-FTIR spectra of the CHI/PSS coated membrane. The carbonyl (C=O) absorption peak of electrospun CA fibrous membrane disappeared after the membrane was coated with CHI and PSS (Figure 4.5 (b) and (c)). It could be due to the deposition of polyelectrolytes which stayed the top of the membrane layer. In Figure 4.5 (b), the characteristic mode of sulfonic groups in PPS was presented at 1,000-1,200 cm^{-1}, SO$_3^-$ symmetric stretching at 1,035 cm^{-1} and benzyl ring at 1,007 cm^{-1}. This finding corresponded well with that of Grumelli et al., 2006 who also examined IR of PSS but with different base membrane. In addition, Figure 4.6 (c) suggests that there could be amino group of CHI at 1,580-1,650 cm^{-1} and the secondary amide at 1,515–1,570 cm^{-1} deposited at the membrane surface. Table 4.3 summarizes the potential functional groups suggested by FTIR result that could exist at the membranes surface.

Table 4.2 Summary of characteristic FTIR peak absorption

Characteristic/assignment	Peak absorption (cm^{-1})
Acetyl group (C=O)	1,747
C-O single bond stretching	1,044 and 1,234
Carboxyl group (COO$^-$)	1,596 and 1,411
Benzyl ring in PSS	1,007
SO$_3^-$ symmetric stretching	1,035
primary amine (-NH$_2$)	1,580-1,650
secondary amide (-CONH)	1,515–1,570

Table 4.3 Potential functional group of the membranes fabricated from this work

Membrane	Functional group			
	Carbonyl (C=O)	Carboxyl (COO-)	Sulfonic (SO$_3$-)	Amino (NH$_2$)
Base e-spun CA fiber	√	-	-	-
CHI/SA$_{15}$	√*	√	-	-
CHI/SA$_{15}$CHI	√*	√	-	√**
CHI/PSS$_{15}$	-	-	√	-
CHI/PSS$_{15}$CHI	-	-	√**	√

* Slight shift in wave length, ** Weak absorption peak
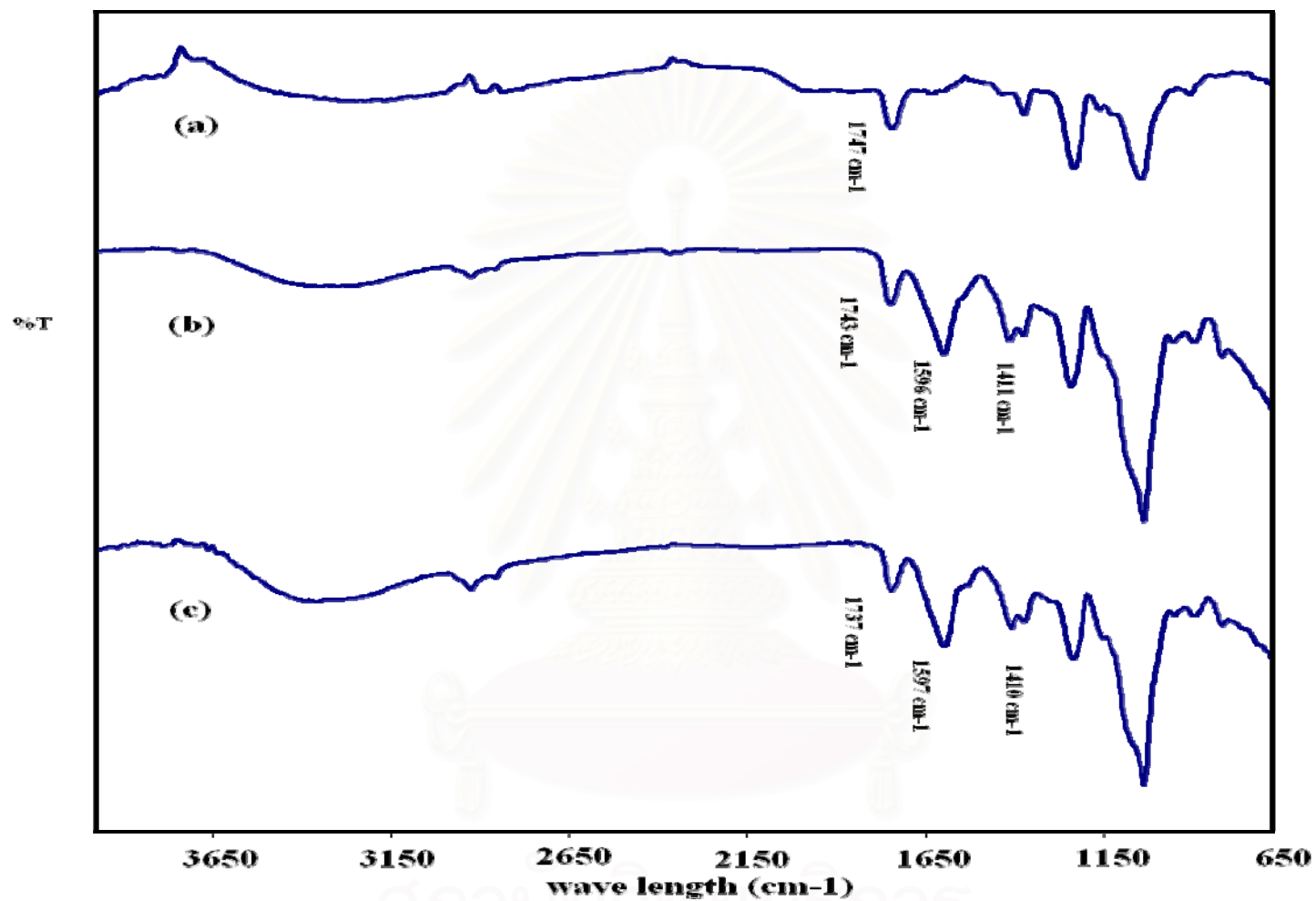
Figure 4.4 HATR-FTIR spectra of (a) base electrospun CA fibrous membrane, (b) with $(CHI/SA)_{15}$ bilayers, and (c) with $(CHI/SA)_{15}CHI$ bilayers
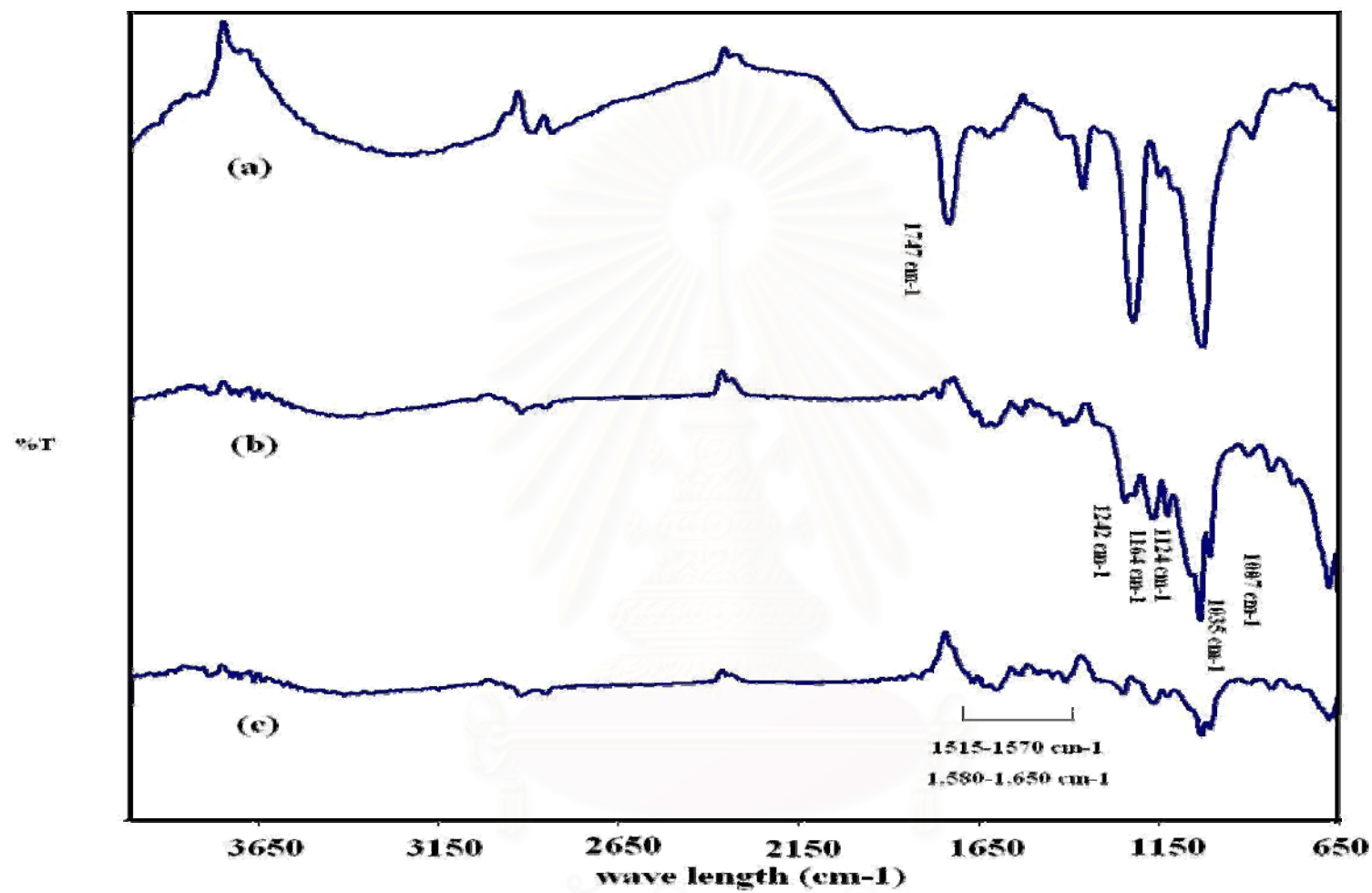
Figure 4.5 HATR-FTIR spectra of (a) base electrospun CA fibrous membrane, (b) with (CHI/PSS)$_{15}$ bilayers, and (c) with (CHI/PSS)$_{15}$CHI bilayers

4.2.3 X-ray photoelectron spectroscopy: XPS

XPS scans were used to confirm the deposit of amino group of CHI on the membrane surface. The elemental scan was carried out for carbon (C) and nitrogen (N). Binding energy of N1s was calibrated with C1s at 285.0 eV. Figure 4.6 shows XPS spectra of N1s. The CA electrospun support did not present the N1s peak and this was consistent with chemical structure. The peak of N1s became weakly apparent at 399 eV after coating the first polyelectrolyte layer of CHI on CA electrospun support (Figure 4.6 (c)). This peak occurred at the same binding energy with that of pure CHI film (which 399.5eV, Figure 4.6 (b)). Therefore CHI could be coated on the CA electrospun support with the fabrication method employed in this work. Figure 4.6 (d) and (e) illustrates the clear peak of N1s for the membrane coated with (CHI/SA)$_{15}$CHI and (CHI/PSS)$_{15}$CHI, where their binding energies were 400 eV and 402.4 eV, respectively. These signals indicated the existence of the polycationic chitosan in multilayer coating.
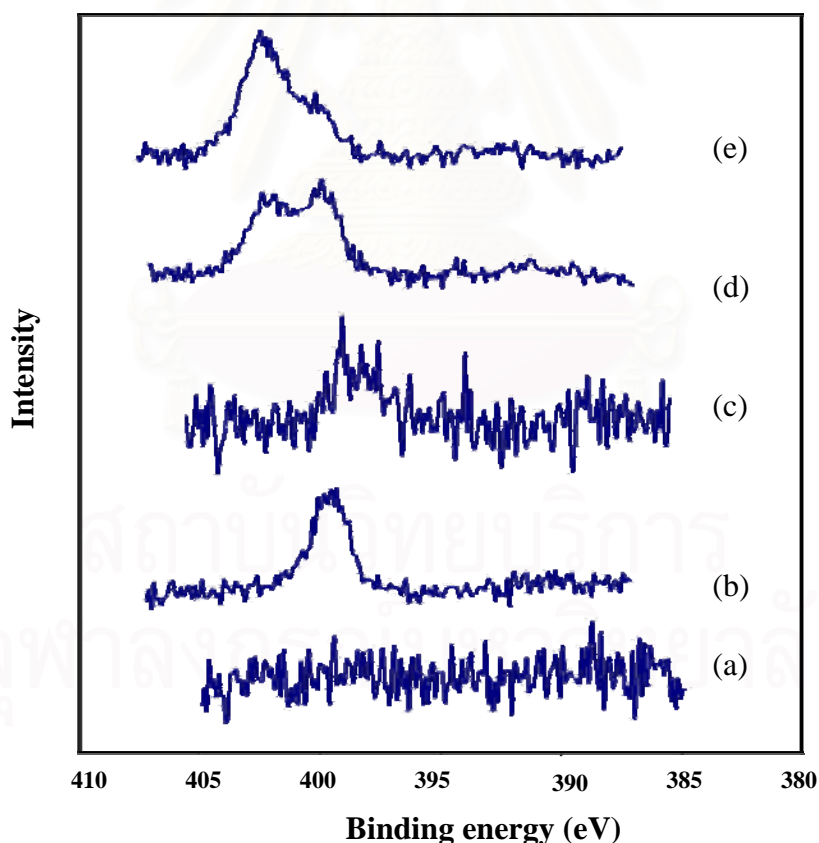
Figure 4.6 XPS spectra of N1s of (a) base electrospun CA fibrous membrane, (b) CHI film, (c) with CHI layer, (d) with (CHI/SA)$_{15}$CHI bilayers, and (e) with (CHI/PSS)$_{15}$ - CHI bilayers

4.2.4 BET analysis

The dip coating of polyelectrolyte solutions as layer by layer on the base electrospun CA fibrous membrane porous support caused the reduction in the surface area as summarized in Table 4.4. This could be because the porous structure of the electrospun CA fibrous were covered or blocked by the polyelectrolyte layers. CHI/SA seemed to exhibit slightly lower surface area then CHI/PSS, but the reason for this still could not be explained with the results obtained from this work.

Table 4.4 Surface area of various membranes

Membrane	Surface area ($m^2\ g^{-1}$)
base CA	8.6
CHI/SA_{20}	5.0
CHI/PSS_{20}	5.7

4.2.5 Thermal property

Figure 4.7 illustrates TGA curves of the $(CHI/SA)_{20}$ coated membranes. When increasing temperature up to $300^{o}C$ the weight of the coated membranes started to and continued to decrease until the temperature reached about $400^{o}C$. Figure 4.8, on the other hand, illustrates that TGA curves of the $(CHI/PSS)_{20}$ coated membranes began to decompose at about $210^{o}C$ and the decomposition continued slowly in the temperature range of $210-440^{o}C$. The composite membranes were more stable than pure polymer materials. Comparison of $(CHI/SA)_{20}$ with $(CHI/PSS)_{20}$ illustrated that the CHI/PSS_{20} coated membrane was more stable than the $(CHI/SA)_{20}$. This could be because PSS had more stable thermal properties than SA and would only start to decompose at about $440^{o}C$.

Figure 4.7 TGA curves of (a) base electrospun CA fibrous membrane, (b) (CHI/SA)$_{20}$ coated membrane, (c) SA film, and (d) CHI film (heating rate of 10°C/min from 50 to 550°C)

Figure 4.8 TGA curves of (a) base electrospun CA fibrous membrane, (b) (CHI/PSS)$_{20}$ coated membrane, (c) CHI film, and (d) PSS film (heating rate of 10°C/min from 50 to 550°C)
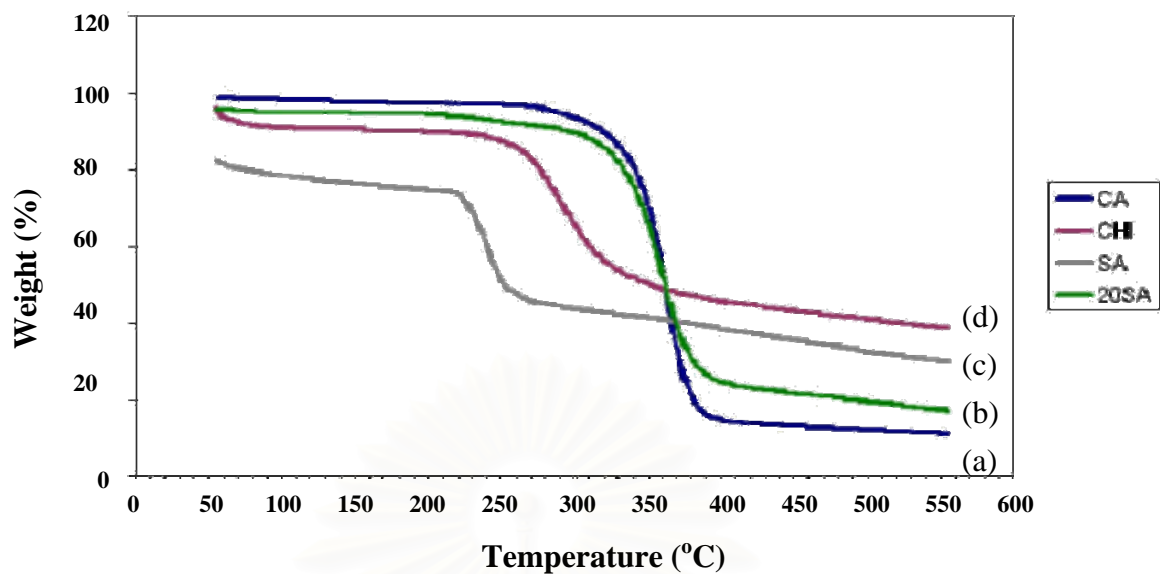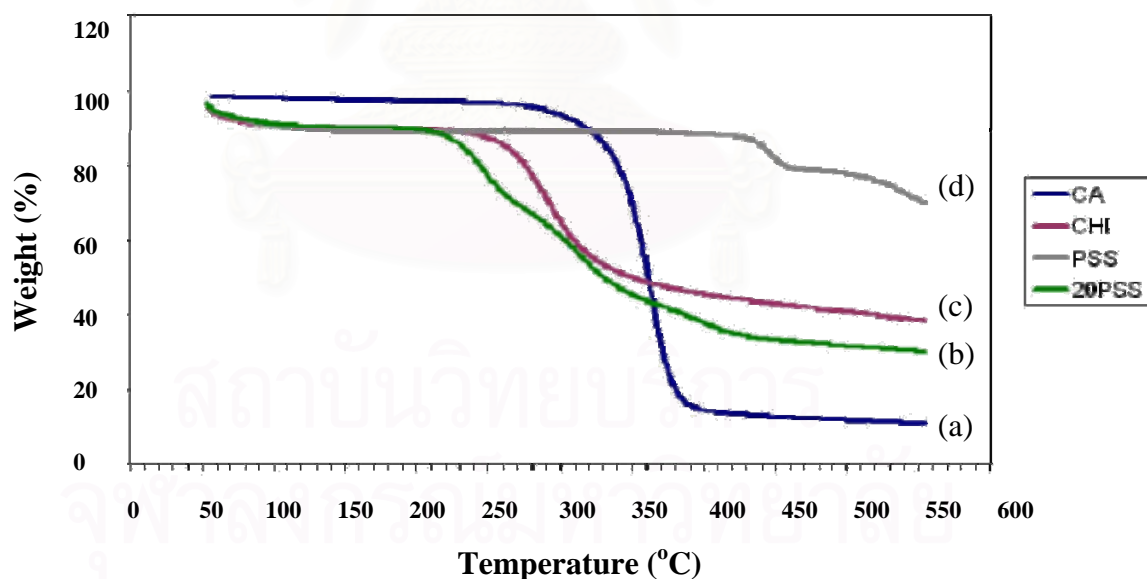
4.3 Desalination

The polyelectrolyte membranes with CHI/SA and CHI/PSS coated on electrospun CA fiber were tested for their desalination performance. The test system was the dead-end filtration unit working at room temperature. The inlet pressure was not controlled (atmospheric pressure) and the outlet was connected to vacuum pump which controlled constant vacuum at 0.3 bar. The membranes were tested for their water permeation flux and salt rejection performance.

4.3.1 Water permeability

The composite membranes were hydrophilic as they contained hydroxyl, carbonyl, carboxyl and amino groups of polymer material structure which are water-soluble and therefore allows the passage of water through the membranes. The base electrospun CA fibrous membrane was highly water-permeable with the flux of about 2,300 L/m^{2}h. The passage of water through this base membrane occured because the pore diameter between interconnecting fibers of ($\sim 1.7 \pm 0.5 \mu$m) was much higher than the size of the mean free path of the water molecule ($\sim 0.1 \mu$m), Lisak et al., 2004. Figure 4.9 depicts the water permeation flux as a function of a number of bilayers which illustrated that the water flux decreased significantly with the number of bilayers. This could be due to the increasing resistance induced by the thicker membrane layer. There were differences between the resistances exerted from the two types of membrane. In the CHI/SA coated membranes, the resistance remained approximately constant when the number of bilayers was below 20, and this increased significantly above 20 layers. On the other hand, the resistance for the CHI/PSS case increased markedly when the number of bilayers increased from 15 to 20, and remained approximately constant after 20 layers. This comparison between the water flux of the two coated membranes demonstrated that CHI/SA and CHI/PSS exerted similar levels of resistance for the water permeation with the water flux of about 40-60 L m^{-2}h^{-1}. The CHI/PSS at 15 bilayers, nevertheless provided an extraordinary level of water flux when compared with the others. It may be that the layer of polyelectrolytes (CHI/PSS) on the base membrane contained a large number of pores both intentional and defected which supported the flow-through of the water.
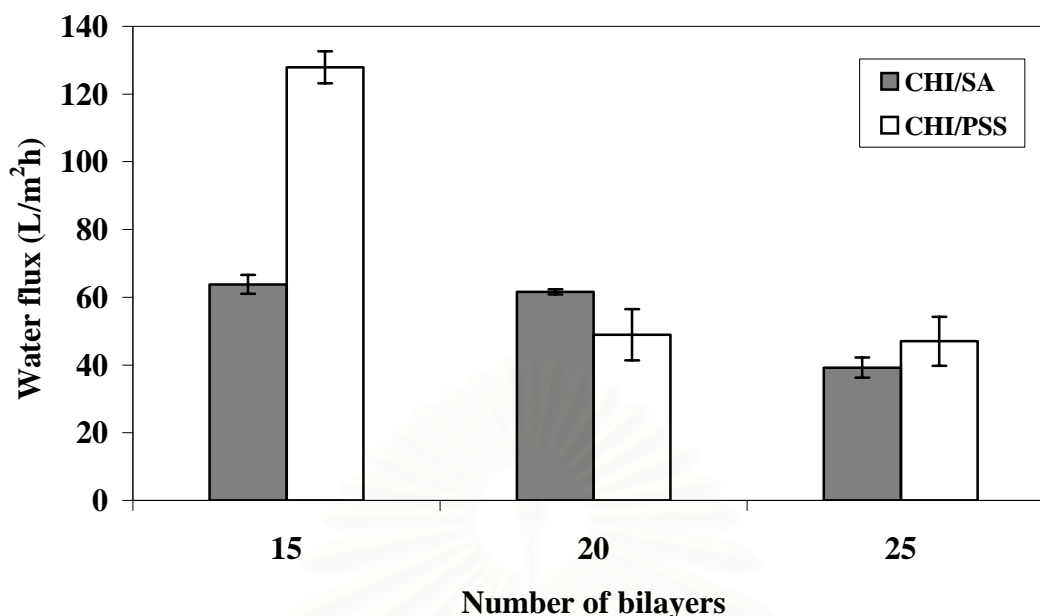
Figure 4.9 Effect of the number of polyelectrolyte bilayers on water flux

4.3.2 NaCl solution separation

The permeation rate of solution and the salt rejection were determined for the coated membrane samples using 2,000 ppm NaCl solution. Figure 4.10 demonstrates the NaCl rejection and the solution flux CHI/SA and CHI/PSS coated membranes. Similar to the water flux results, the NaCl solution flux decreased with an increase in the number of bilayers which could be due to an increase in the thickness of polyelectrolyte layer with the number of bilayers as stated above. However, the flux obtained from the NaCl solution was less than the water flux (with no NaCl). This could be due to the effect of osmotic pressure which counteracted the vacuum driving force for the water passage according to reduce net pressure driving (see Table 4.5).

The rejection of NaCl increased substantially with the number of bilayers. A proposed mechanism for the rejection of NaCl from the membrane is as follows:
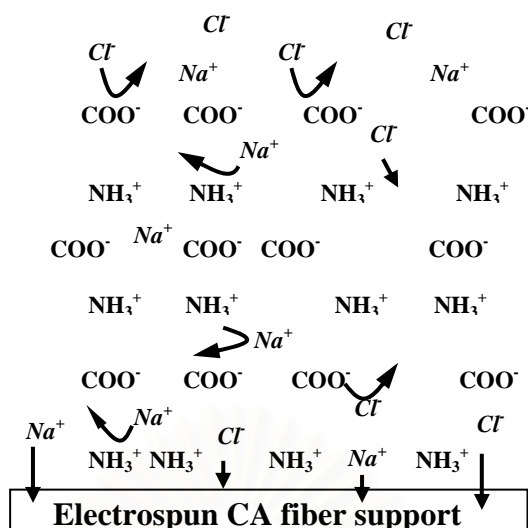
where NH_3^+ and COO^- (or SO_3^-) are active functional groups of CHI and SA (or PSS), respectively. In this mechanism which Na^+ and Cl^- could be counter ions with charge polyelectrolytes layer. A thicker membrane consisted of higher number of amino, carboxyl and sulfonic groups which could be distributed more properly throughout the membrane. This acted as a barrier for the movement of NaCl through the membrane layer.

In this experiment, the two membranes did not provide significantly different results regarding the salt rejection (see Table 4.5), despite of the SEM results which indicated that CHI/SA had a denser surface than the CHI/PSS coated membrane. It could be that CHI, SA, and PSS were low charge density (the number carbon atoms per repeating unit is taken as a measure for the charge density) (Haack et al., 2001). Thus the capacities of the two membranes in retarding the movement of NaCl were similar.

Table4.5 Comparison of water flux, %NaCl rejection, and NaCl solution flux of different polyanionic membranes (20 bilayers)

membrane	water flux $(L\ m^{-2}\ h^{-1})$	%NaCl rejection*	NaCl solution flux* $(L\ m^{-2}\ h^{-1})$	$(\Delta P - \Delta \pi)^{**}$ (bar)
CHI/SA$_{20}$	61.6±0.7	9.7±0.4	47.4±1.6	0.53
CHI/PSS$_{20}$	48.9±7.6	8.7±0.9	38.4±3.0	0.55

* experiments with NaCl solution at 2,000 ppm,

** $\Delta P - \Delta \pi$ equal to net pressure driving force
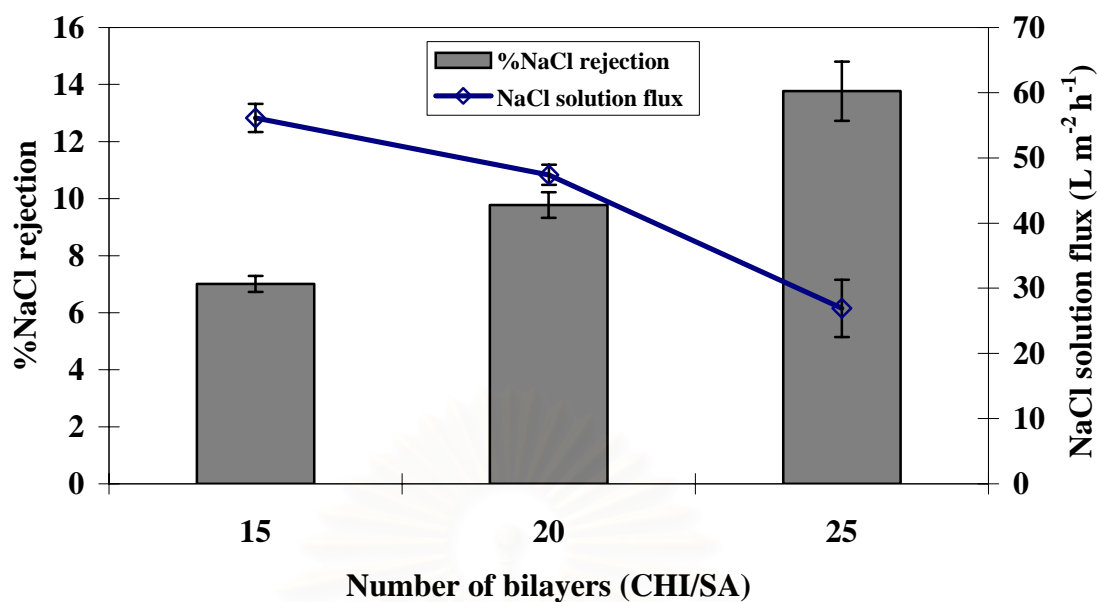
(a)
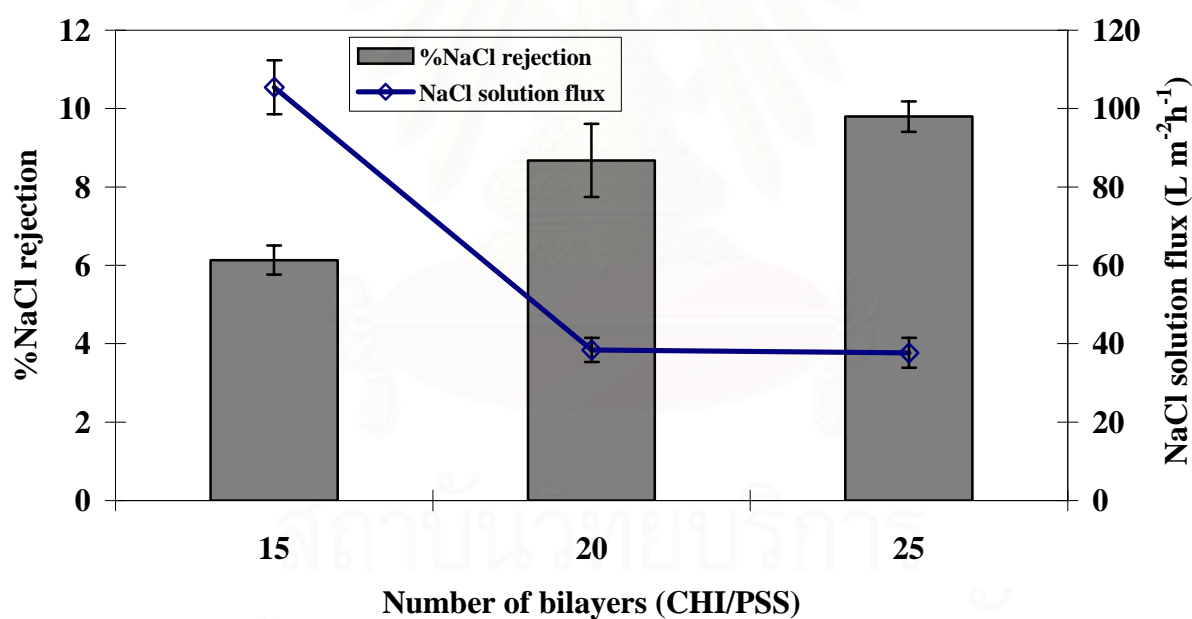
(b)

Figure 4.10 Effect of the number of polyelectrolyte bilayers on NaCl rejection and NaCl solution flux: (a) CHI/SA and (b) CHI/PSS coated membranes

Table 4.6 displays the comparisons of water fluxes from this work and those reported in literature. In this comparison, the membrane fabricated in this work

performed reasonably well in providing high water fluxes. However, the NaCl rejection from these membranes was quite low compared to literature (see Table 4.7). As the CHI/SA membrane was quite dense, the water passage through the membrane must have come from the dissolution of NaCl into the membrane material, or otherwise the water permeability should have occurred due to the defect in the membrane material. For the CHI/PSS membrane, the membrane seemed to contain a large number of holes distributed on the surface of the membrane. SEM suggested that this pore diameter was quite large (in the magnitude of 10^{-6} m) which was on the different scale with the size of Na^+ (which was about 3×10^{-10} m).

Table4.6 Comparison of water flux among the various membranes

support (technique)	coated polyelectrolytes	the number of bilayers	water flux (L/m^2h)	condition of permeation test	reference
CA (electrospinning)	CHI/SA	25	23.8	under vacuum pressure	this work
CA (phase inversion)	CHI/SA	25	19.2	operating pressure 16 bar	Lajimi et al, 2004
PAN /PET (oxygen plasma)	PVA/PVS	60	3.8	operating pressure 40 bar	Toutianoush et al., 2005

Table4.7 Comparison of %NaCl rejection among the various membranes

support /technique	coated polyelectrolytes	the number of bilayers	NaCl concentration (ppm)	%NaCl rejection	condition of permeation test	reference
CA (electrospinning)	CHI/SA	25	2000	13	under vacuum pressure	this work
CA (phase inversion)	CHI/SA	25	1989	75	operating pressure 16 bar	Lajimi et al, 2004
PAN /PET (oxygen plasma)	PVA/PVS	60	585	93	operating pressure 40 bar	Toutianoush et al., 2005

4.3.3 Effect of NaCl concentration

Figure 4.11 illustrates the effect of NaCl concentration on desalination with the CHI/SA$_{20}$ coated membranes and it was found that NaCl solution flux decreased with increasing NaCl concentration (Figure 4.11 (a)), as would be expected from an

increasing osmotic pressure drop across the membrane. In this experiment, it was assumed NaCl concentration of the permeate was equal to that in the flask. The osmotic pressure is related linearly with salt concentration following Vant Hoff equation (Mulder, 1996):

$$\pi = C_i RT / M_i \qquad (4.1)$$

where π is osmotic pressure (Pa)

C_i is solution concentration by mass (g/ m^3)

R is gas constant (8.314 Pa m^3/mole K)

T is absolute temperature (298 K)

M_i is molecular weight of solute (g/mole)

The net pressure driving force is $\Delta P - \Delta \pi$ where ΔP equal to pressure difference across the membrane (0.7 bar) and $\Delta \pi$ equal to osmotic pressure difference across the membrane (see Table 4.8). For the range of conditions examined in this work, ΔP was constant, whereas $\Delta \pi$ increased with salt concentrations. Hence, the net pressure driving force decreased with salinity. In this experiment, the effect of the osmotic pressure became more pronounced at NaCl concentration of 3,000 ppm.

Table 4.8 Pressure difference with NaCl concentration

NaCl concentration (ppm)	ΔP (bar)	$\Delta \pi$ (bar)	$\Delta P - \Delta \pi$ (bar)
1,000	0.7	0.04	0.66
2,000	0.7	0.17	0.53
3,000	0.7	0.49	0.21

In addition, increasing salt concentration could induce concentration polarization on the membrane surface, and this also could retard the solution flux. On the contrary, %NaCl rejection increased with NaCl concentration. This was unexpected as an increase in NaCl concentration should have enhanced the dissolution of NaCl into the membrane resulting in a higher NaCl being transported through the membrane. However, in this case, as the dissolution of NaCl into the

membrane should be quite low. Preliminary results illustrated that the partition of NaCl into the membrane was negligible and therefore the effect of dissolution should be minimal. For this case, an increase in NaCl concentration caused the polarization at the membrane surface and therefore reduced the flux and increased the subsequent salt selectivity. Hence, an increase in the %NaCl rejection was observed.
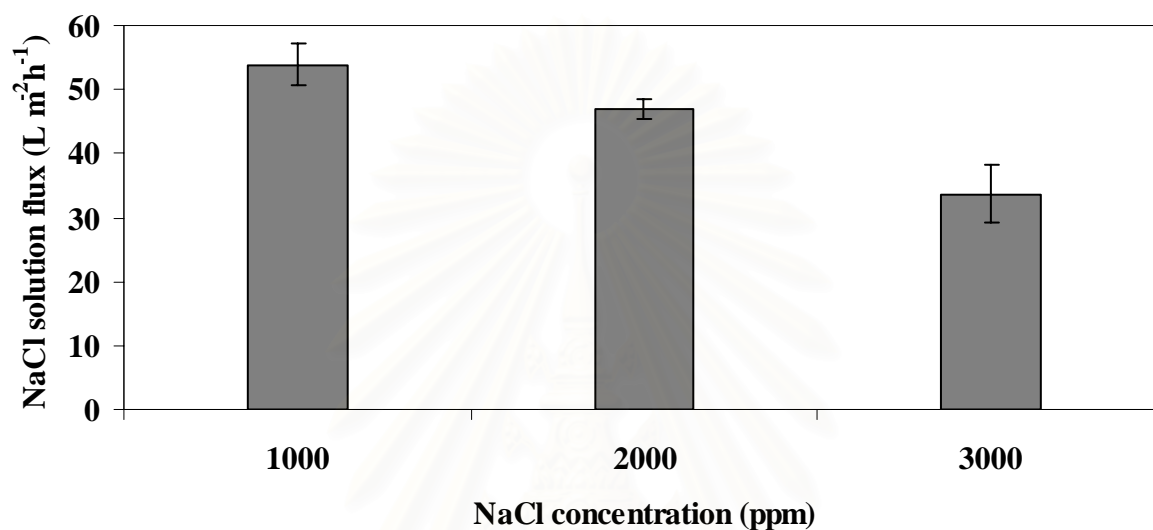
(a)
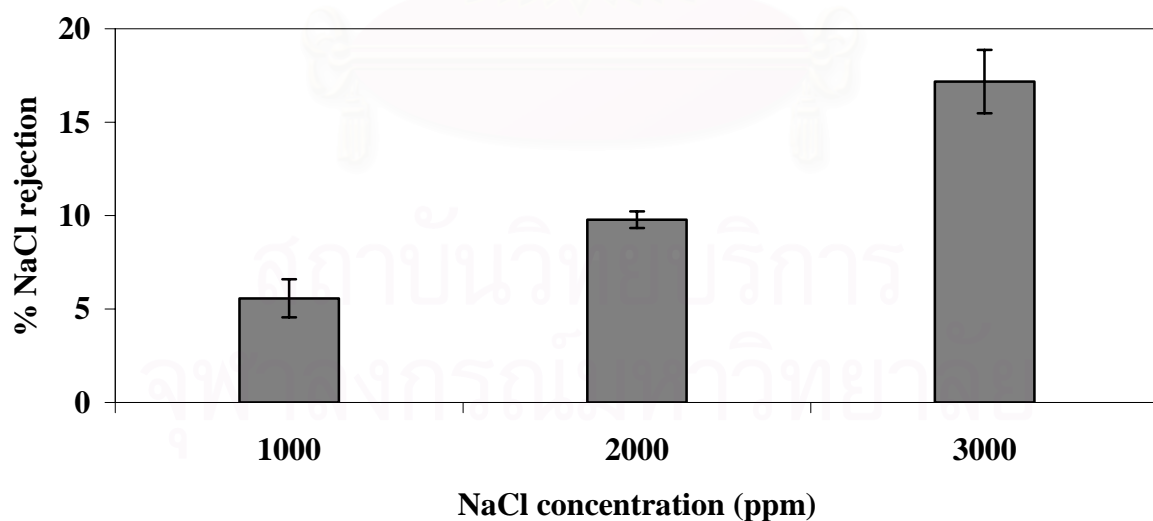
(b)

Figure 4.11 Effect of NaCl concentration on NaCl rejection: (a) NaCl solution flux, and (b) NaCl rejection with $(CHI/SA)_{20}$ coated membranes

CHAPTER V
CONCLUSIONS AND RECOMMENDATIONS

5.1 Conclusions

Major findings from this work include:

- The base electrospun CA fibrous membrane was successfully coated with polyelectrolytes multilayers (polycationic: chitosan (CHI), polyanionic: sodium alginate (SA) and poly (styrene sulfonate) sodium salt (PSS)) to form composite membrane.

- Physical appearances morphology of the CHI/SA coated membrane was denser than the CHI/PSS coated membrane.

- The main functional groups of the coated membrane were carboxyl and sulfonic groups of SA and PSS, respectively, whereas the CHI/SA membrane only showed slight appearance of amino groups from CHI structure.

- XPS spectra confirmed the deposition of amino groups from CHI on multilayer membrane surface.

- The pure water flux through both types of membrane in the range of 60 L m^{-2} h^{-1} for 15 bilayers and 40 L m^{-2} h^{-1} for 25 bilayers and this decreased significantly with an increase in the number of bilayers.

- NaCl solution flux was lower than pure water flux due to the effect of osmotic pressure and this decreased with increasing NaCl concentration.

- The rejection of NaCl increased substantially with the number of bilayers of the polyelectrolytes multilayers which was in the range of 15 % for 25 bilayers and 6 % for 15 bilayers.

- The composite membranes, at this stage, would not be suitable for actual desalination process but will be suitable for ultrafiltration or microfiltration process.

5.2 Contributions

This research illustrates the advantages of electrospinning technique to generate to the base membrane of composite membrane with high porosity due to non-woven fiber structure. The high porosity is suitable for separation applications as it could provide high water fluxes. The top layer was made of composite multilayer biopolymers which were thin to minimize the resistance and the technique employed in this work successfully generated a thin layer of composite membranes (CHI/SA and CHI/PSS) on the surface of the base electrospun. This method is economical with no hazardous waste generated and the resulting membrane provided good pure water fluxes. However, it still could not give high desalination properties due potentially to the defect and the "not-so-good" hydrophobic nature of the membrane. The membrane might therefore be used in a pretreatment of the sea water before using conventional reverse osmosis technique to desalinate the sea water.

5.3 Recommendations / Future works

Based on the preliminary results of this study, some recommendations for future studies are proposed.

1. The composite membranes should be investigated for properties such as thermal stability, long term stability, and mechanical property.

2. More in-depth quantitative analysis for the amount active functional groups on membrane surface should be conducted.

3. There are still other parameters can affect top layer the fabrication such as polyelectrolyte concentration, pH of polyelectrolyte solution, type and molecular weight of polyelectrolyte. These should be investigated.

4. New technique for single-sided coating method should be developed to reduce the membrane resistances.

5. In actual membranes, the top layers of the membrane should be coated onto a strong support such as high porosity ceramic membrane to enhance the durability of the membrane product.

6. The effect of shear rate on the cross-flow filtration unit should also be examined.

REFERENCES

Baker, R.S. 2004. Membrane technology and applications. 2 nd ed. England: John Wiley & Sons.

Ferjani, E., Lajami, R.H., Deratani, A., and Roudesli, M.S. 2002. Bulk and surface Modification of cellulose diacetate based RO/NF membranes by polymethylhydrosiloxane. Preparation and characterization. Desalination 146: 325-330.

Ferjani, E., Roudesli, S., and Deratani, A. 2004. Desalination of brackish water from Tunisian Sahel using composite polymethylhydrosiloxane-cellulose acetate membranes. Desalination 162: 103-109.

Grumelli , D., Bonazzola , C., and Calvo, E.J. 2006. Hydration cycling in redox active LBL self-assembled polyelectrolyte multilayers. Electrochemistry Communications 8: 1353–1357

Haack, J.M., Lenk, W., Lehmann, D., and Lunkwitz, K. 2001. Pervaporation separation of water/alcohol mixtures using composite membranes base on polyelectrolyte multilayer assemblies. Journal of Membrane Science 184: 233-243

Haddad, R., Ferjani, E., Roudesli, M.S., and Deratani, A. 2004. Properties of cellulose acetate nanofiltration membranes. Application to brackish water desalination. Desalination 167: 403-409.

Hong, S.U., Malaisamy, R., and Bruening, M.L. 2006. Optimization of flux and selectivity in Cl^-/SO_4^{2-} separations with multilayer polyelectrolyte membranes. Journal of Membrane Science 283: 366-372.

Hong, S.U., Malaisamy, R., and Bruening, M.L. 2007. Separation of Fluoride from other monovalent anions using mutilayer polyelectrolyte nanofiltration membranes. Langmuir 23: 1716-1722.

Jiraruttananont, R. 1998. Synthetic membrane separation process. 2 nd ed. Bankok: Thaiseng press.

Lajimi, R.H., Abdallah, A.B., Ferjani, E., Roudesli, M.S., and Deratani, A. 2004. Change of the performance properties of nanofiltration cellulose acetate membranes by surface adsorption of polyelectrolyte multilayers. Desalination 163: 193-202.

Lisak, D., Rusciano, G., and Sasso, A. 2004. An accurate comparison of lineshape models on H$_2$O lines in the spectral region around 3 µm. journal of Molecular Spectroscopy 227: 162-171.

Ma, Z., Kotaki, M., and Ramakrishna, S. 2005. electrospun cellulose nanofiber as affinity membrane. Journal of Membrane Science 265: 115-123.

Mulder, M. 1996. Basic Principle of Membrane Technology. Kluwer Acedemic Publishers.

Park, J.S., Lee, C.M., and Lee, K.Y. 2007. A surface plasmon resonance biosensor for detecting *Pseudomonas aeruginosa* cells with self-assembled chitosan-alginate multilayers. Talanta 72: 859-862.

Roh, I.J., Greenberg, A.R., and Khare, V.P. 2006. Synthesis and characterization of interfacially polymerized polyamide thin films. Desalination 191: 279-290.

Stanton, B.W., Harris, J.J., Miller, M.D., and Brueng, M.L. 2003. Ultrathin, multilayered polyelectrolyte film as nanofiltration membranes. Langmuir 19: 7038-7042.

Suntarapha, K., 2004. Membrane separation technology. Bankok: cuprint.

Toutianoush, A., Jin, W.J., Deligoz, H., and Tieke, B. 2005. Polyelectrolyte multilayer membranes for desalination of aqueous salt solutions and seawater under reverse osmosis conditions. Applied Surface Science 246: 437-443.

Tungprapa, S., Jangchud, I., and Supaphol, P. 2007. Release characteristic of four model drugs from drug-loaded electrspun cellulose acetate fiber mats. Polymer 48: 5030-5041.

Wang, T., Turhan, M., and Gunasekaran, S. 2004. Select properties of pH-sensitive, biodegradable chitosan-poly (vinyl alcohol) hydrogel. Polymer International 54: 911-918

Wang, X., Fang, D.,Yoon, K., Hsiao, B.S. and Chu, B., 2006. High performance ultrafiltration composite membranes based on poly (vinyl alcohol) hydrogel coating on crosslinked nanofibrous poly (vinyl alcohol) scaffold. Journal of Membrane Science 278: 261-268.

Yeom, C.K., Kim, C.U., Kim, B.S., Kim, K.J., and Lee, J.M. 1998. Recovery of anionic surfactant by RO process. Preparation of polyelectrolyte-complex anionic membrane. Journal of Membrane Science 143: 207-218.

APPENDIX

APPENDIX

- Solution properties

- Chitosan solution at 0.4 %w/v in acetic acid 1%vol.

Property	value
Conductivity	1024 µs/cm
pH	3.6
Viscosity	30.9+/-1.2 cP
	(at 105 rpm, 26 ^{o}C, and %torque 53.9)

- Sodium alginate solution at 1 % w/v in water

Property	value
Conductivity	2.27 ms/cm
pH	6.4
Viscosity	44.6+/-0.7 cP
	(at 120 rpm, 25.5 ^{o}C, and %torque 89.2)

- Poly (sodium 4-styrenesulfonate) solution at 0.4 % w/v in water

Property	value
Conductivity	1644 µs/cm
pH	4.3
Viscosity	4.1+/-0.8 cP
	(at 140 rpm, 29.3 ^{o}C, and %torque 9.5)

- Correlation between conductivity and concentration of NaCl solution

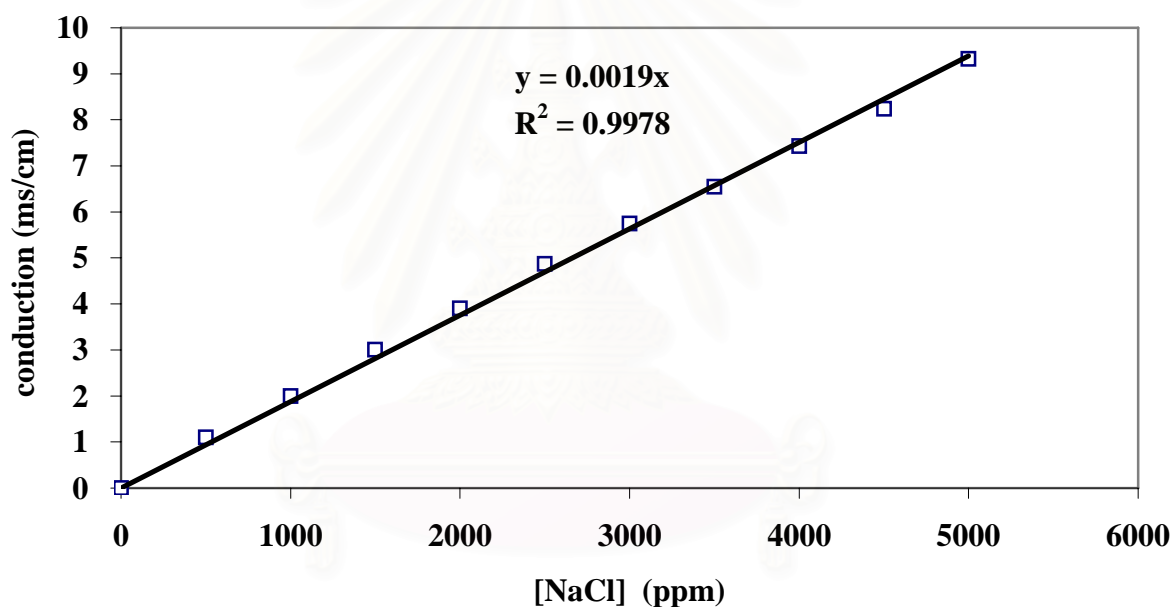| [NaCl] (ppm)	Conduction (ms/cm)
500	1.10
1,000	2.00
1,500	3.01
2,000	3.90
2,500	4.87
3,000	5.75
3,500	6.55
4,000	7.43
4,500	8.24
5,000	9.33

Fig.1-A Standard curve plot between conductivity and concentration of NaCl solution

Therefore the correlation between conductivity and concentration of NaCl solution following in this equation

$$\mu = 0.0019 \, C \qquad \text{(1-A)}$$

where, μ is conductivity of NaCl solution

C is NaCl concentration

- Molecular weight of Chitosan (CHI) by GPC

Instrument: Gel Permeation Chromatography (GPC), PL-GPC 110

Test condition:

 Eluent: acetate buffer

 Flow rate: 0.6 mL/min

 Injection volume: 20 µL

 Temperature: 30 ^{o}C

 Column set: Ultrahydrogel linear 1 column + guard column

 Polymer standard: Polysaccharide standard kits

 Calibration method: Polysaccharide standard calibration

   (MW 5,900-788,000)

 Detector: Refractive Index Detector

GPC result

Mn	Mw	Mp	Mz	Mz+1	Polydispersity
325,380	1,258,515	639,648	3,532,390	6,456,620	3.87

- Molecular weight of sodium alginate (SA) by GPC

Instrument: Gel Permeation Chromatography (GPC), Water 600E

Test condition:

      Eluent: sodium bicarbonate buffer (pH 11)

      Flow rate: 0.6 mL/min

      Injection volume: 20 µL

      Temperature: 30 $^{\circ}$C

      Column set: Ultrahydrogel linear 1 column (MW resolving range = 1,000-

            20,000) 1 column + guard column

      Standard: Pullulans (MW 5,900-788,000)

      Calibration method: Polysaccharide standard calibration

      Detector: Refractive Index Detector

Sample preparation: Samples (2 mg/mL) were dissolved in eluent and filtered using nylon 66 membrane (pore size 0.45 µm) before injection.

GPC result

Mn	Mw	Mp	Mz	Mz+1	Polydispersity
218,931	721,216	354,696	1,819,725	3,199,600	3.29

- Osmotic pressure

In this experiment, it was assumed NaCl concentration of the permeate was equal to that in the flask. The osmotic pressure is following Vant Hoff equation (Mulder, 1996):

$$\pi = nC_iRT / M_i \qquad (2\text{-}A)$$

where π is osmotic pressure (Pa)

C_i is NaCl solution concentration by mass (g/ m^3)

R is gas constant (8.314 Pa m^3/mole K)

T is absolute temperature (298 K)

M_i is molecular weight of solute (58.5 g/mole)

n is number of ion (equal to 2 for NaCl)

C_1 (ppm)	C_2 (ppm)	π_1 (Pa)	π_2 (Pa)	$\Delta\pi$ (Pa)	$\Delta\pi$ (bar)
1,000	948	84,703	80,298	4,405	0.04
2,000	1,798	169,406	152,296	17,110	0.17
3,000	2,423	254,110	205,236	48,874	0.49

1 and 2 represent in permeate and flask, respectively.

- TGA analysis

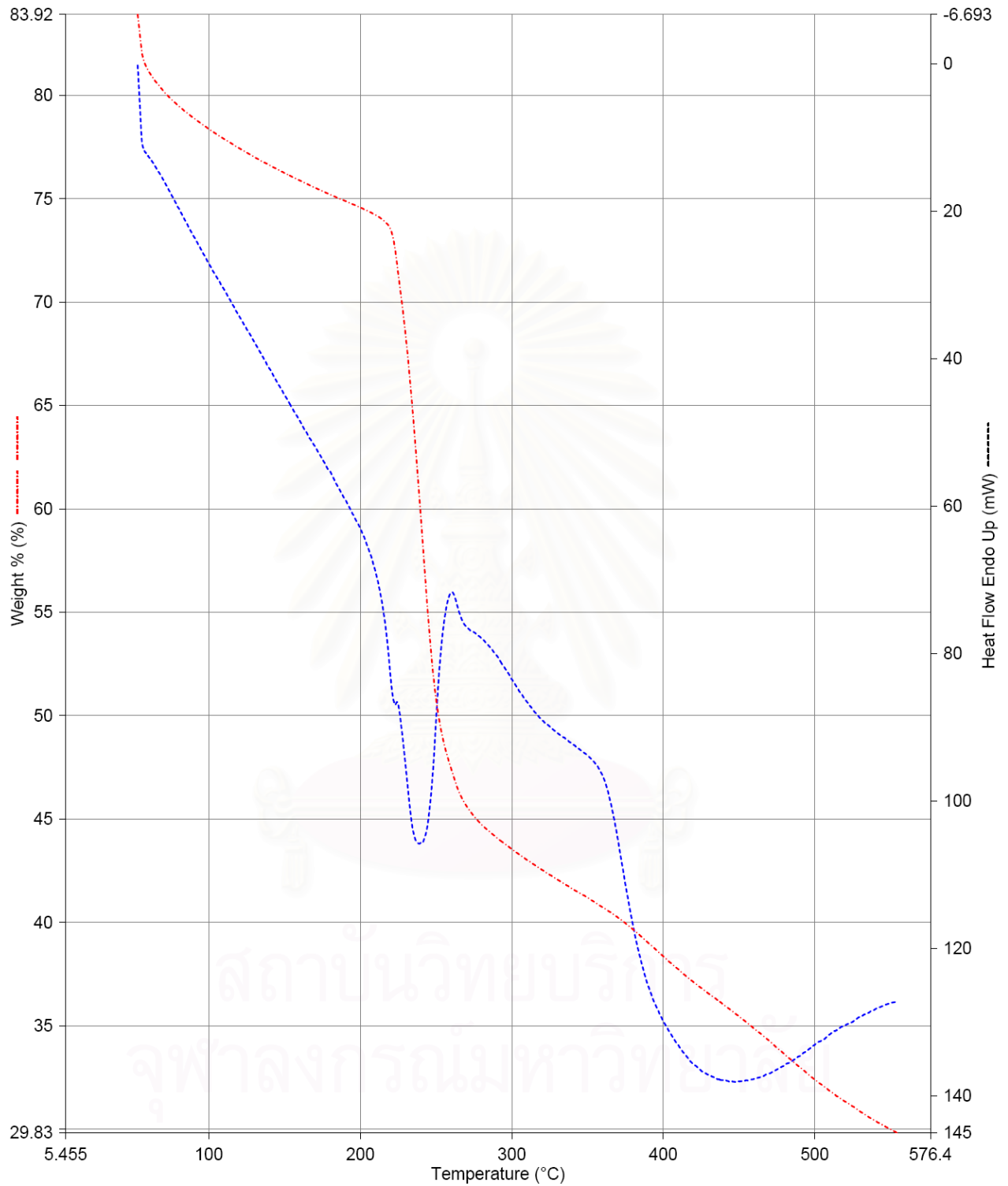**Condition:** - Hold for 1 min at 50 $^{\circ}$C

- Heat from 50 to 550 $^{\circ}$C at 10 $^{\circ}$C/min

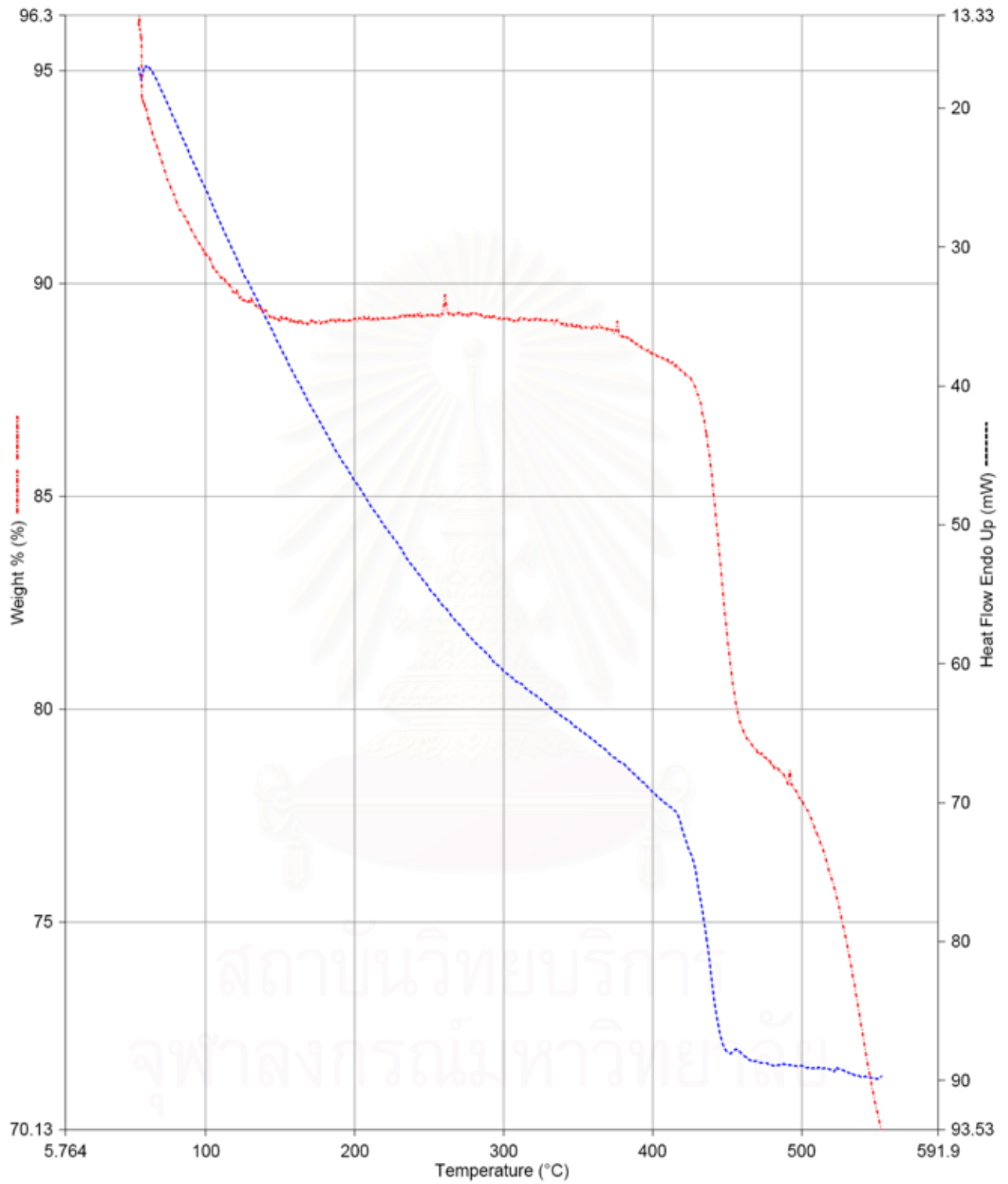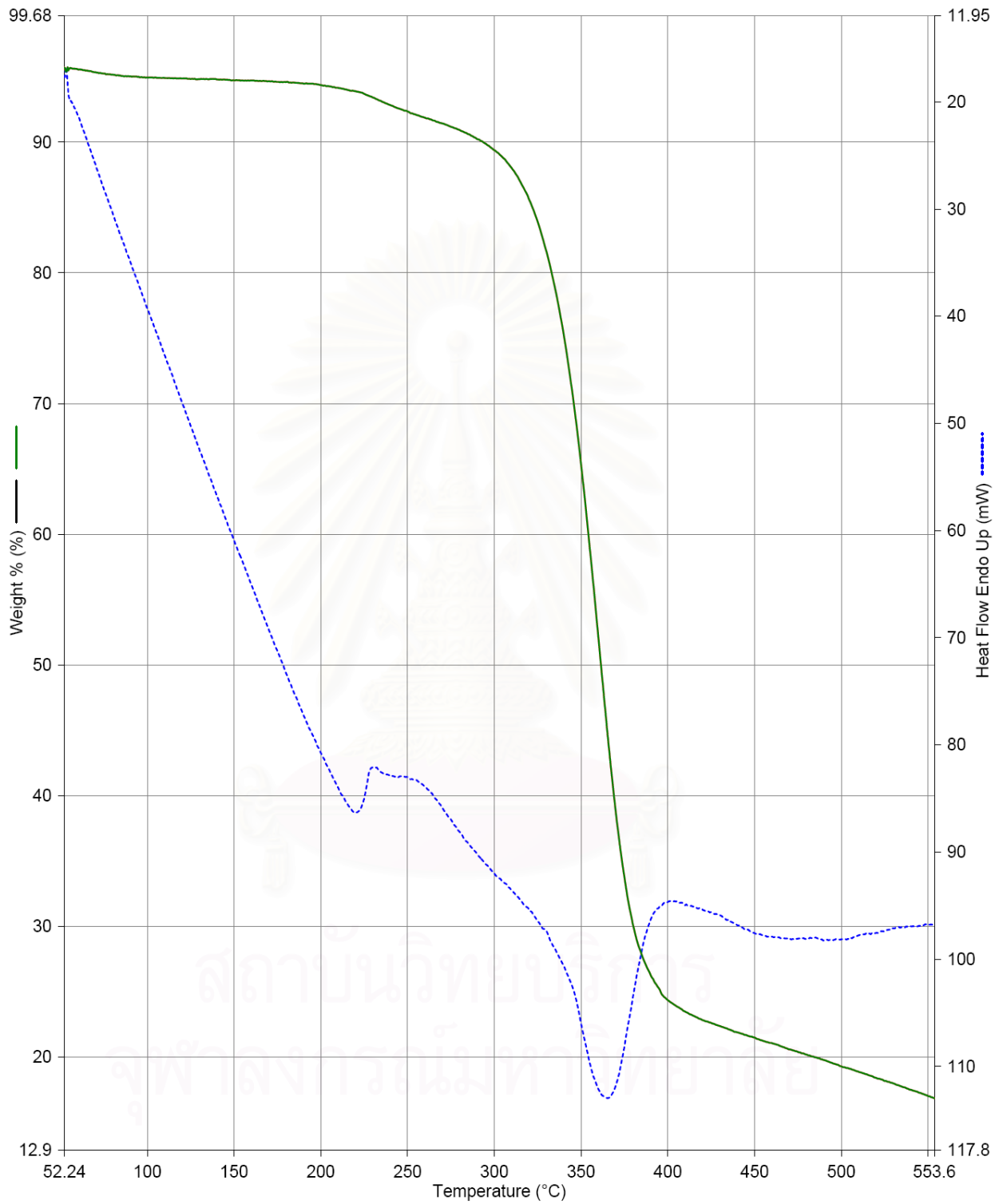1) Cellulose acetate
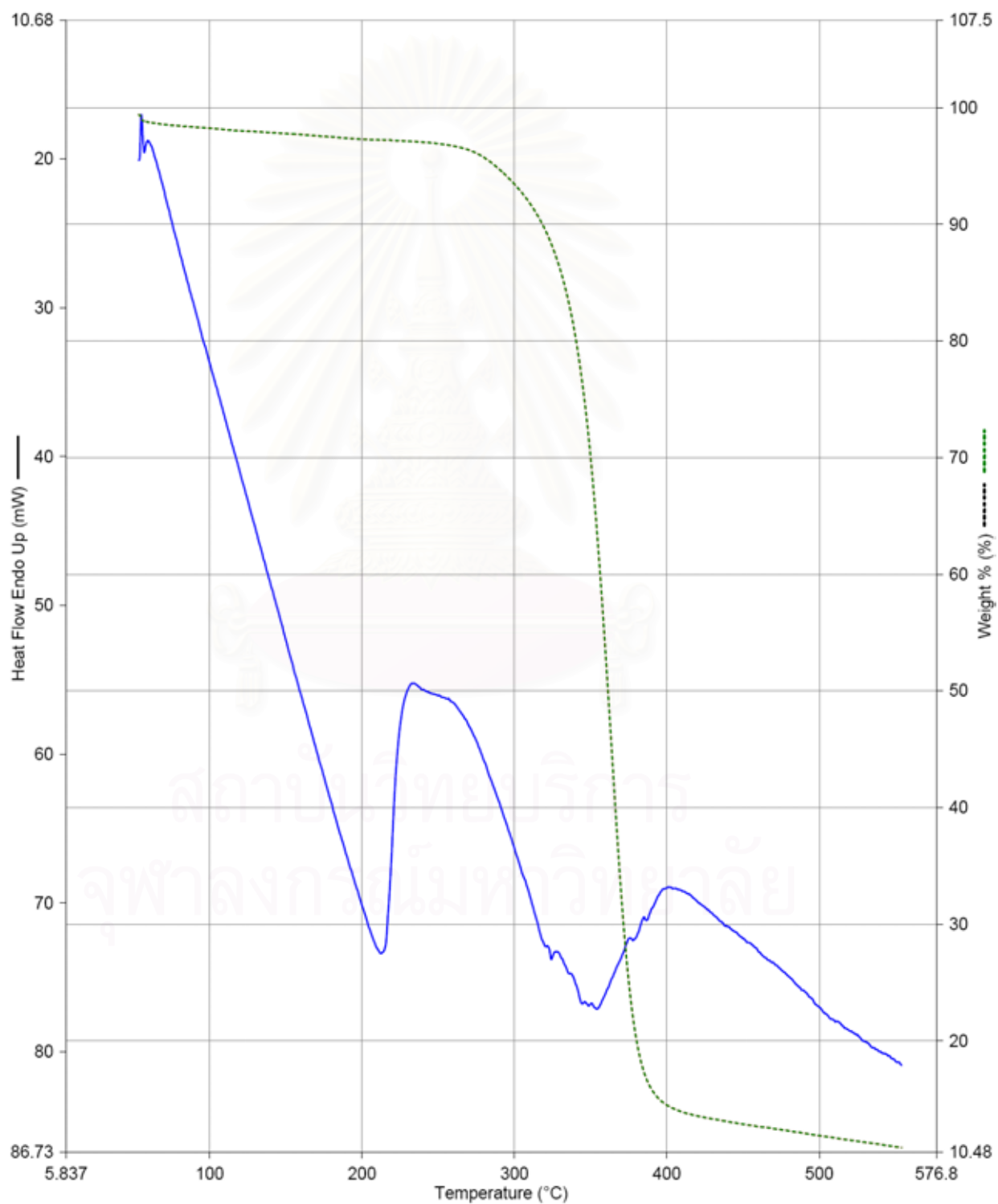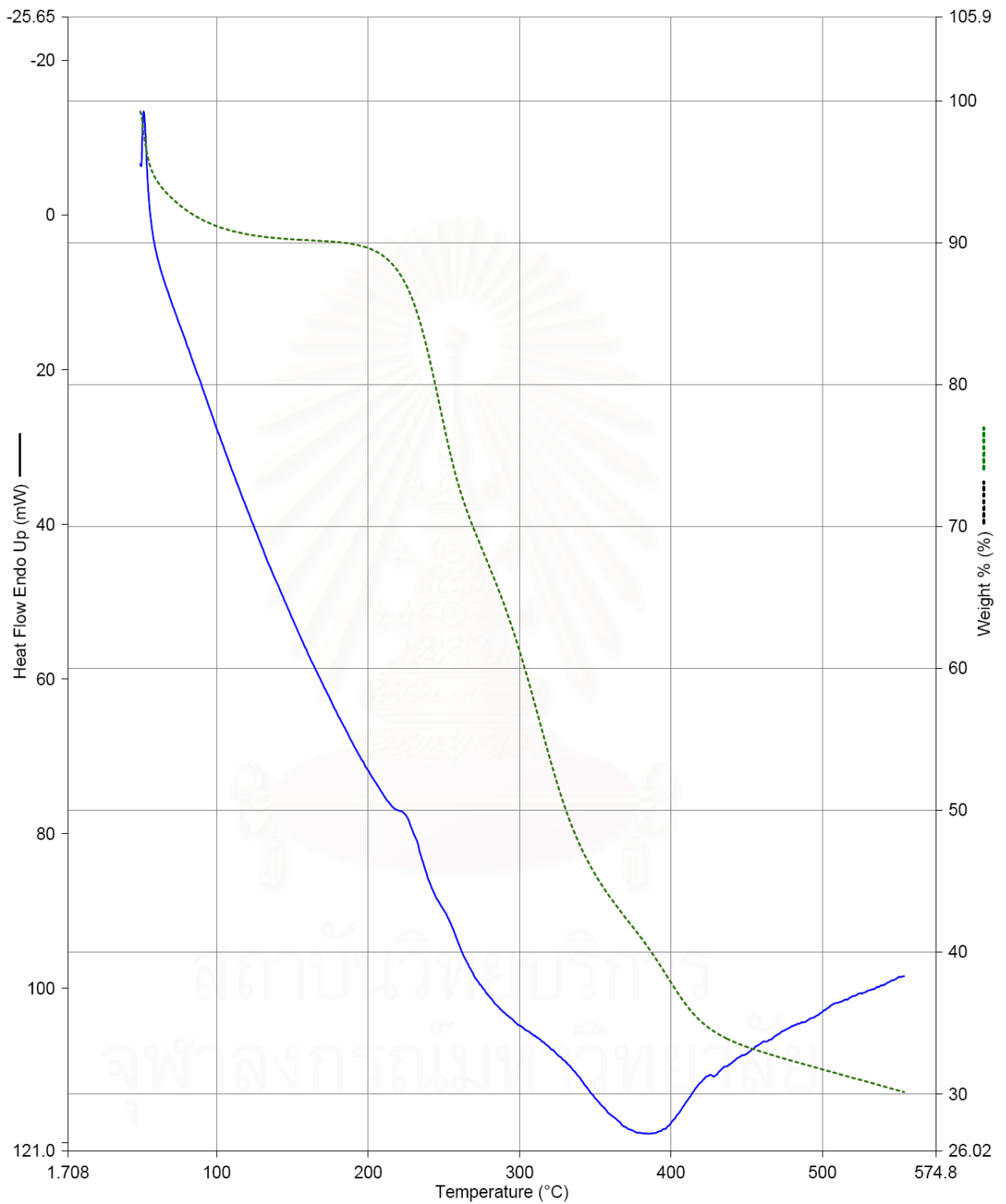
2) Chitosan
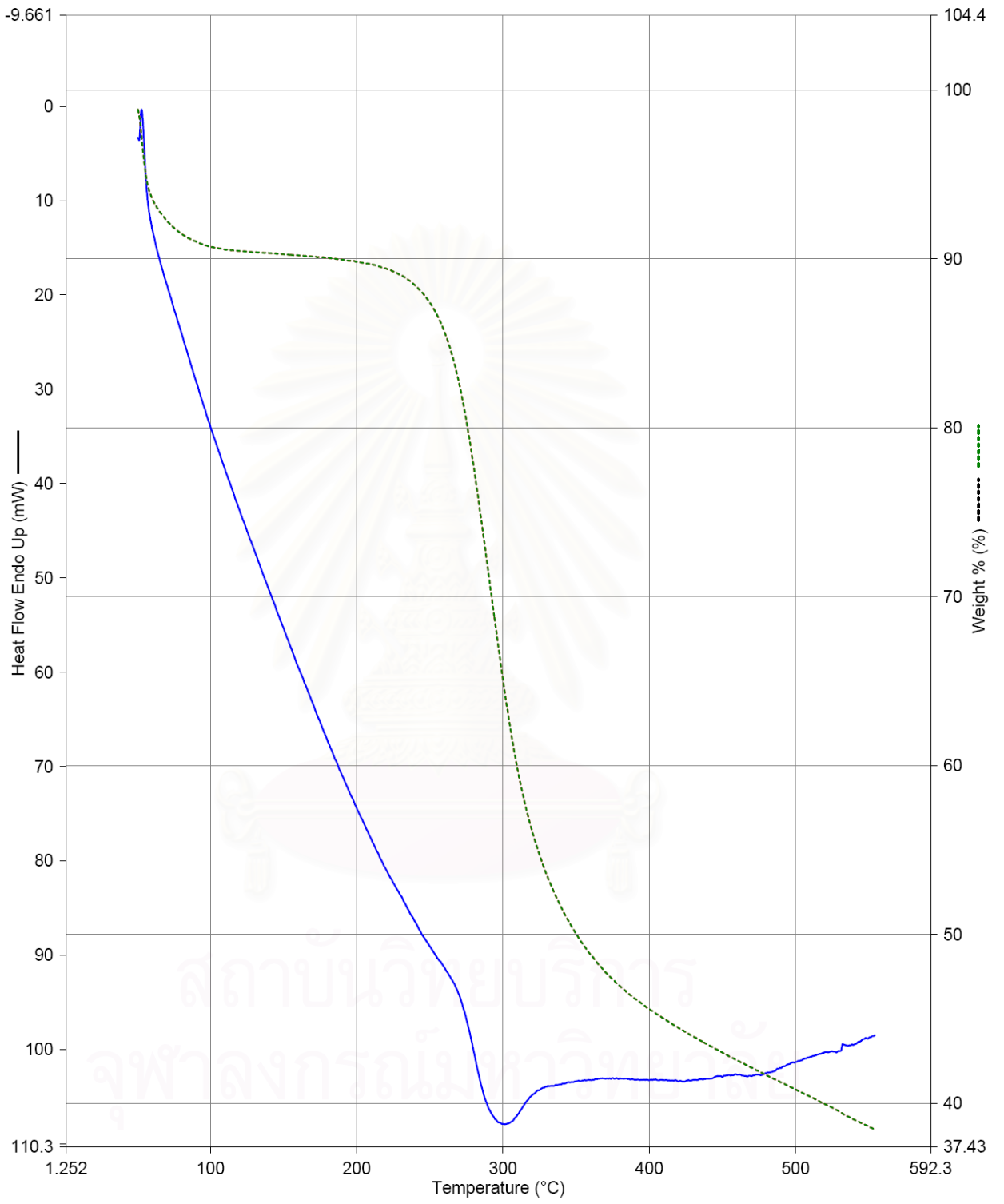
3) Sodium alginate

4) Poly (styrene sulfonate) sodium salt

5) (CHI/SA)$_{20}$ coated membrane

6) (CHI/PSS)$_{20}$ coated membrane

BIOGRAPHY

Miss Watadta Ritcharoen was born on 3rd November, 1983 in Chachoengsao. She finished her secondary course from Benchamaradcharungsarit School in March, 2001. After that, she studied in the major of Industrial Chemistry in Faculty of Science at King Monkut's Institute of Technology Ladkrabang. She continued her further study for Master's degree in Chemical Engineering at Chulalongkorn University. She participated in the Biochemical Engineering Research Group and achieved her Master's degree in April, 2008.